Check for updates

Microbial Biotechnology

WILEY

MICROBIAL BIOTECHNOLOGY Open Access

RESEARCH ARTICLE OPEN ACCESS

Adaptive Laboratory Evolution Rewires *Pseudomonas putida* for Resource-Efficient Acetate Assimilation

Nicolás Gurdo[1] | Aparajitha Srinivasan[2,3] | Tommaso Tagliani[1] | Melanie Filbig[4] | Nicolas T. Wirth[1] | Josefin Johnsen[1] | Garret W. O'Connell[1] | Stefano Donati[1] | Enrico Orsi[1] | María V. G. Alván-Vargas[1] | Yan Chen[2,3] | Christopher J. Petzold[2,3] | Matthew Blow[5] | Thomas Eng[2,3] | Till Tiso[4,6] | Lars M. Blank[4,7] | Adam Feist[1,2,8] | Aindrila Mukhopadhyay[2,3,9] | Pablo I. Nikel[1]

[1]BRiGHT, Technical University of Denmark, Kgs. Lyngby, Denmark | [2]Joint BioEnergy Institute, Emeryville, California, USA | [3]Biological Systems and Engineering Division, Lawrence Berkeley National Laboratory, Berkeley, California, USA | [4]Institute of Applied Microbiology, RWTH Aachen University, Aachen, Germany | [5]U.S. Department of Energy Joint Genome Institute, Berkeley, California, USA | [6]Systems Biotechnology, Technical Faculty, Bielefeld University, Bielefeld, Germany | [7]WSS Research Centre "CatalAix", Aachen, Germany | [8]Department of Bioengineering, University of California San Diego, La Jolla, California, USA | [9]Environmental Genomics and Systems Biology Division, Lawrence Berkeley National Laboratory, Berkeley, California, USA

Correspondence: Pablo I. Nikel (pabnik@dtu.dk)

Received: 21 August 2026 | **Revised:** 5 October 2026 | **Accepted:** 12 October 2026

Keywords: acetate | adaptive laboratory evolution | metabolic engineering | metabolism | multi-omic analyses | *Pseudomonas putida* | synthetic biology

ABSTRACT

Acetate is an attractive renewable two-carbon substrate for microbial biotechnology, but toxicity limits growth and carbon-use efficiency at process-relevant concentrations. Here, we used adaptive laboratory evolution to improve acetate tolerance in a genome-reduced strain of *Pseudomonas putida* and combined whole-genome sequencing, quantitative physiology, reverse engineering, transcriptomics, proteomics and ^{13}C-acetate fluxomics to resolve the underlying adaptation mechanisms. Evolution under increasing acetate concentrations selected recurrent mutations in *gacA* and *fabB*, which encode a global response regulator and a fatty acid biosynthesis enzyme, respectively. Reverse engineering of these mutations recapitulated most of the evolved phenotype, including shorter lag phase and substantially higher biomass yield from acetate. Multi-omic analyses showed repression of type VI secretion systems, carbohydrate storage functions, fatty acid metabolism and oxidative stress-associated proteins, indicating resource reallocation away from costly stress and non-essential programs. Fluxomics further revealed reduced carbon cycling and increased glyoxylate shunt flux, consistent with improved acetate-carbon retention in biomass. These results establish acetate tolerance in *P. putida* as a resource-efficiency phenotype and identify *gacA* and *fabB* as actionable targets for acetate-based bioproduction.

1 | Introduction

Microbial bioproduction increasingly relies on alternative carbon sources to reduce feedstock costs and improve sustainability (Schrader et al. 2009; Dürre and Eikmanns 2015; Wendisch et al. 2016; Kiefer et al. 2021). Acetate is an attractive two-carbon (C_2) substrate as it is relatively inexpensive and can be generated through several renewable routes, including biomass hydrolysis, syngas fermentation and microbial electrosynthesis (May et al. 2016; Lim et al. 2018; Novak and Pflügl 2018; Zhang et al. 2024). Acetate also constitutes a useful entry point into metabolism because it can be directly converted into acetyl-coenzyme A (CoA) (Luli and Strohl 1990; Kim et al. 2021), a central precursor for growth and biosynthesis. However, acetate toxicity limits its use at process-relevant concentrations (Kuang et al. 2024). As a weak organic acid, acetate can impair cytosolic

This is an open access article under the terms of the Creative Commons Attribution-NonCommercial-NoDerivs License, which permits use and distribution in any medium, provided the original work is properly cited, the use is non-commercial and no modifications or adaptations are made.

© 2026 The Author(s). *Microbial Biotechnology* published by John Wiley & Sons Ltd.

pH homeostasis, disrupt central metabolism, increase maintenance demands and reduce microbial fitness (Roe et al. 1998; Lasko et al. 2000; Chong et al. 2013; Trček et al. 2015; Pinhal et al. 2019). Accordingly, extracellular pH is a major determinant of acetate toxicity that dictates the relative abundance of protonated acetic acid (CH_3COOH) and dissociated acetate (CH_3COO^-) (Bakker and Mangerich 1983). As such, changes in acetate concentration and pH during cultivation should be considered together when interpreting acetate-tolerance phenotypes. A mechanistic understanding of these complex responses is therefore needed to exploit acetate more effectively in microbial cell factories.

Pseudomonas putida is a robust platform for bioproduction because it can tolerate diverse environmental and chemical stresses (Nikel and de Lorenzo 2014, 2018; Volke, Calero, and Nikel 2020; Volke, Friis, et al. 2020; Weimer et al. 2020), including organic acids (de Lorenzo et al. 2024). Genome-reduced variants of *P. putida* KT2440 have been developed as streamlined hosts for heterologous expression and metabolic engineering (Lieder et al. 2015; Volke, Calero, and Nikel 2020; Volke, Friis, et al. 2020; Wirth, Funk, et al. 2023; Wirth, Rohr, et al. 2023; Bushin et al. 2026). Genome reduction can remove dispensable genetic elements and decrease the burden associated with non-essential functions (Calero and Nikel 2019; Wynands et al. 2019; Ma et al. 2024), thereby improving genetic stability and freeing cellular resources for product formation (Yus et al. 2009). These properties motivated the selection of the genome-reduced strain SEM1.4 as a production-oriented background for improving growth on and tolerance to acetate. Identifying beneficial adaptations in this *chassis* could provide targets for further development of acetate-based bioproduction processes.

Acetate uptake in *P. putida* KT2440 occurs through the acetate permease ActP, followed by conversion into acetyl-CoA by acetyl-CoA synthetase (Acs). Acetyl-CoA can then enter the tricarboxylic acid (TCA) cycle, the glyoxylate shunt, lipid metabolism, or biosynthetic routes, depending on the physiological state of the cell. Previous engineering strategies have improved acetate utilisation in Gram-negative bacteria by modifying endogenous metabolic pathways, including the glyoxylate shunt, or by targeting regulatory nodes across central metabolism, for example, through modulation of isocitrate lyase activity (Díaz-Guerra et al. 1997; Roe et al. 2002; Seong et al. 2020). Recent work has also examined acetate use as a mixed carbon source with glucose in *P. putida* (Viana de Siqueira et al. 2025), and this C_2 substrate is typically used as an energy source in selection schemes for synthetic one-carbon assimilation (Puiggené et al. 2025; Turlin et al. 2025). Despite substantial progress in this domain, acetate toxicity remains a barrier to efficient growth and production, with rates, yields and titres often remaining below values required for industrial implementation.

Adaptive laboratory evolution (ALE) offers a complementary route to improve substrate tolerance and uncover the genetic basis of complex phenotypes. ALE enriches beneficial mutations under defined selective pressures and has been widely used to improve growth, stress resistance, substrate uptake and production traits (Dragosits and Mattanovich 2013; Choe et al. 2019; Fernández-Cabezón et al. 2019; Sandberg et al. 2019). An example of such a framework is the adaptation of *Escherichia coli* to acetate as a carbon source. Sandberg et al. (2017), for instance, evolved *E. coli* MG1655 on minimal medium containing acetate, nearly doubling the specific growth rate from 0.27 to 0.43 h^{-1} and increasing acetate uptake from 12 to 20–23 mmol g cell dry weight (CDW) $^{-1}$ h^{-1}. Furthermore, when combined with multi-omic analyses, ALE can reveal how adaptation propagates across regulatory, metabolic and physiological layers. Hence, integrating whole-genome sequencing, transcriptomics, proteomics and fluxomics enables a systems-level view of genotype–phenotype relationships and exposes cellular strategies that support tolerance to specific stresses (Horinouchi and Furusawa 2020).

Here, we applied ALE to a genome-reduced *P. putida* strain under gradually increasing acetate concentrations. We isolated acetate-tolerant clones, performed whole-genome sequencing to identify mutations associated with acetate adaptation, reverse-engineered key mutations into the parental background and integrated transcriptomics, proteomics and ^{13}C-based fluxomics to elucidate the mechanisms underlying acetate tolerance. This approach identified mutations in *gacA* and *fabB* as key contributors to the evolved phenotype and revealed systems-level changes in secretion systems, fatty acid metabolism, methionine and polyamine catabolism, iron uptake and central carbon fluxes. Together, these analyses define genetic and metabolic targets for improving acetate assimilation in *P. putida* cell factories.

2 | Materials and Methods

2.1 | Bacterial Strains, Plasmids and Culture Conditions

Strains and plasmids used in this study are listed in Tables S1 and S2, respectively. *E. coli* DH5α *λpir* was used as the cloning host for genetic manipulations. *E. coli* strains were cultivated at 37°C, and *P. putida* strains were cultivated at 30°C. Routine cloning, genome engineering and strain propagation were performed in lysogeny broth (LB, 10 g L^{-1} tryptone, 5 g L^{-1} yeast extract and 10 g L^{-1} NaCl). Liquid precultures were grown in 50-mL Falcon centrifuge tubes containing 10 mL of medium. Shaken-flask cultivations were performed in 250-mL baffled Erlenmeyer flasks containing 50 mL of medium. Liquid precultures were incubated at 250 rpm in a MaxQ 8000 incubator (Thermo Fisher Scientific Inc., Waltham, MA, USA), while shaken-flask cultures were incubated at 200 rpm in a New Brunswick Innova 42R shaker (Eppendorf SE, Hamburg, Germany). Solid media contained 15 g L^{-1} agar. Whenever required, kanamycin (Km) or gentamicin (Gm) was added at 50 or 10 μg mL^{-1}, respectively.

For ALE, clone screening, phenotypic characterisation and multi-omic experiments, strains were cultivated in minimal salt medium (MSM), modified from Hartmans et al. (1989), containing 3.88 g L^{-1} K_2HPO_4, 1.63 g L^{-1} NaH_2PO_4, 2 g L^{-1} $(NH_4)_2SO_4$, 0.1 g L^{-1} $MgCl_2{\cdot}6H_2O$, 10 mg L^{-1} ethylenediaminetetraacetic acid (EDTA), 2 mg L^{-1} $ZnSO_4{\cdot}7H_2O$, 1 mg L^{-1} $CaCl_2{\cdot}2H_2O$, 5 mg L^{-1} $FeSO_4{\cdot}7H_2O$, 0.2 mg L^{-1} $Na_2MoO_4{\cdot}2H_2O$, 0.2 mg L^{-1} $CuSO_4{\cdot}5H_2O$, 0.4 mg L^{-1} $CoCl_2{\cdot}6H_2O$ and 1 mg L^{-1} $MnCl_2{\cdot}2H_2O$ (Turlin et al. 2022) buffered with 5 g L^{-1} 3-(*N*-morpholino)propanesulphonic acid (MOPS, 24 mM). Potassium acetate was added at the concentrations indicated below, and the medium

17517915, 2026, 10, Downloaded from https://environmicro-journals.onlinelibrary.wiley.com/doi/10.1111/1751-7915.70459 by Universitatsbibliothek RWTH Aachen University, Wiley Online Library on [13/11/2026]. See the Terms and Conditions (https://onlinelibrary.wiley.com/terms-and-conditions) on Wiley Online Library for rules of use; OA articles are governed by the applicable Creative Commons License

pH was adjusted to 7.0 after acetate addition. Across all acetate conditions tested, the medium pH before adjustment typically ranged from 6.9 to 7.1. Under the 100 mM acetate conditions used for physiological characterisation, this formulation limited the increase in culture pH to 7.6–7.8 at the mid-exponential sampling points, although a constant pH was not maintained throughout cultivation. Culture pH was periodically monitored during and at the end of cultivation in selected experiments. To inoculate experimental cultures, aliquots from precultures were harvested by centrifugation at 8000 × *g* for 5 min at room temperature, washed with MSM without a carbon source, and resuspended in the final experimental medium to the desired starting optical density at 600 nm (OD_{600}).

2.2 | Adaptive Laboratory Evolution (ALE) on Acetate

ALE of *P. putida* SEM1.4 was performed in 250-mL baffled Erlenmeyer flasks containing 50 mL of buffered MSM and supplemented with potassium acetate (otherwise indicated as acetate for simplicity). Three parallel evolution experiments were initiated at 20 mM acetate, and the substrate concentration was increased stepwise to 180 mM. At each concentration, cultures were incubated at 30°C and 200 rpm until they reached mid-exponential phase (OD_{600}~0.5). Then, 500 μL of culture was transferred into fresh medium. In some cases, the transfer was done at the same acetate concentration for two additional passages before increasing acetate concentration further. The evolution experiment lasted 130 days, corresponding to ca. 200 passages, and was terminated when no further growth improvement was observed.

2.3 | Screening of Evolved Populations and Isolation of Clones

The final evolved populations from the three parallel ALE lineages were plated separately on MSM agar containing 180 mM acetate. Ten colonies with different colony sizes were selected from these plates, purified by repeated streaking and stored at −80°C in a cryopreservation solution containing 50% (*v*/*v*) glycerol, 0.1 M $MgSO_4$ and 50 mM Tris·HCl (pH = 8). Phenotypic screening of selected clones was done in a Growth Profiler 960 system (Enzyscreen BV, Heemstede, The Netherlands) using square 96-well microtiter plates sealed with gas-permeable sandwich covers (Enzyscreen BV). MSM containing 5 g L^{-1} MOPS and supplemented with acetate at 20, 60, 100, 140, or 180 mM was inoculated at an initial OD_{600} of 0.1 in a final volume of 300 μL per well. Bacterial growth was monitored every 15 min by optical image scanning in the Growth Profiler apparatus. G-values, corresponding to integrated green values obtained from each scan and well, were transformed into equivalent OD_{600} values using calibration curves fitted to a Monod function (Equation 1):

$$G - \text{value} = a \times OD_{600} / \left(b + OD_{600}\right) \quad (1)$$

The parameters *a* and *b* were determined by non-linear regression. For calibration, the OD_{600} of serial culture dilutions in MSM was measured in a UV-1600PC spectrophotometer (VWR Inc., Radnor, PA, USA), and the corresponding images were acquired in the Growth Profiler apparatus. Following phenotypic screening, clone 6 from lineage 1 was selected for downstream physiological and systems-level analyses based on its robust growth at high acetate concentrations. This isolate was designated *P. putida* SEM1.4^{Evo}.

2.4 | Whole-Genome Sequencing

Genomic DNA was extracted from cultures using the PureLink Genomic DNA Mini Kit (Thermo Fisher Scientific Inc., Waltham, MA, USA). Sequencing libraries were prepared using PlexWell (seqWell Inc., Beverly, MA, USA), and sequencing was performed on a NextSeq 500 instrument (Illumina Inc., San Diego, CA, USA) with an Illumina NextSeq mid-output kit using 300 cycles. Sequencing files were analysed with an in-house pipeline described previously (Phaneuf et al. 2019), based on Bowtie2 (Deatherage and Barrick 2014), using the *P. putida* KT2440 reference genome (Belda et al. 2016) with GenBank accession number AE015451. Average sequencing coverage was ca. 60× for clonal and population samples. For population samples, mutations with frequencies < 0.5 were excluded from the analysis (LaCroix et al. 2017; Calero et al. 2022) to filter out potential artefacts and to focus on mutations enriched during ALE.

2.5 | Reverse-Engineering of Mutations in *P. putida* SEM1.4

Point mutations identified during ALE were introduced into the parental strain by homologous recombination-mediated gene replacement. Uracil-excision (USER) cloning (Cavaleiro et al. 2015) was used to construct all plasmids. USER oligonucleotide primers containing the targeted single-nucleotide substitutions were designed with AMUSER (Genee et al. 2015) and are listed in Table S3. Phusion *U* Hot Start DNA Polymerase (Thermo Fisher Scientific Inc.) was used for PCR amplification, mutagenesis and construction of USER-compatible DNA fragments. PCR products were analysed on 1% (*w*/*v*) agarose gels and purified with the NucleoSpin Gel and PCR Clean-up kit (Macherey-Nagel GmbH, Düren, Germany). Purified amplicons were assembled into plasmid pSNW2 (Volke, Calero, and Nikel 2020; Volke, Friis, et al. 2020) using USER enzyme (New England BioLabs Inc., Ipswich, MA, USA) according to the manufacturer's instructions, and the resulting plasmids were transformed into *E. coli* DH5α λ*pir* by heat shock (Nikel et al. 2008). Gene replacement was performed using I-*SceI*-mediated recombination (Wirth et al. 2020) with inducible self-curing vectors (Volke, Calero, and Nikel 2020; Volke, Friis, et al. 2020). Positive clones, screened by green fluorescence and colony PCR, were grown in LB. Cultures were washed with 0.3 M sucrose and transformed by electroporation with the self-curing helper plasmid pQURE6·H (Wirth, Funk, et al. 2023; Wirth, Rohr, et al. 2023). Cells were recovered overnight in LB containing 5 mM 3-methylbenzoate and then streaked onto LB agar containing Gm and 5 mM 3-methylbenzoate. Gene substitution events were screened by red fluorescence, colony PCR and DNA sequencing. Single colonies were then grown in LB without selection to cure the helper plasmid. Non-fluorescent colonies were selected, and plasmid loss was verified by colony

17517915, 2026, 10, Downloaded from https://environmicro-journals.onlinelibrary.wiley.com/doi/10.1111/1751-7915.70459 by Universitatsbibliothek RWTH Aachen University, Wiley Online Library on [13/11/2026]. See the Terms and Conditions (https://onlinelibrary.wiley.com/terms-and-conditions) on Wiley Online Library for rules of use; OA articles are governed by the applicable Creative Commons License

PCR, parallel plating on LB or LB and Gm, and DNA sequencing. Confirmed mutants were grown in LB and preserved as cryostocks.

2.6 | Phenotypic Characterisation of Reverse-Engineered Strains

The parental strain *P. putida* SEM1.4, the acetate-evolved strain SEM1.4^{Evo}, and the reverse-engineered strain SEM1.4 GacA^{E197K} FabB^{L77P}, together with other control strains indicated in the text, were phenotypically characterised in 250-mL baffled Erlenmeyer flasks containing 50 mL of MSM containing 5 g L^{-1} MOPS and supplemented with 100 mM acetate. This acetate level was the lowest concentration that clearly differentiated the strains in microplate experiments. Cultures were inoculated at an initial OD_{600} of 0.1 and incubated at 30°C and 200 rpm. OD_{600} was measured during cultivation, and acetate consumption was quantified by high-performance liquid chromatography (HPLC). Samples were centrifuged at 10,000 × *g* for 5 min at 4°C, and supernatants were stored at −20°C until HPLC analysis. CDW was determined under the same cultivation conditions. For this, six 10-mL samples were collected per strain at different cultivation times, corresponding to two samples per biological replicate, in pre-weighed 15-mL Falcon tubes. OD_{600} was measured before sample processing. Biomass was harvested by centrifugation at 8000 × *g* for 10 min at 4°C and washed twice with MSM without a carbon source. Tubes containing the biomass were frozen at −20°C and lyophilised under vacuum until constant weight. Growth parameters were derived from these measurements using the QurvE software (Wirth, Funk, et al. 2023; Wirth, Rohr, et al. 2023).

2.7 | Metabolite Analysis

Acetate consumption was analysed using a Dionex UltiMate 3000 HPLC system (Thermo Fisher Scientific Inc.) equipped with an Aminex HPX-87H ion-exclusion column (300 × 7.8 mm, Bio-Rad Laboratories Ltd., Hercules, CA, USA), a refractive index detector, and UV detectors set to 210, 260, 277 and 304 nm (Nikel and de Lorenzo 2013; Federici et al. 2025). The column was maintained at 45°C, and samples were eluted with 5 mM H_2SO_4 at a constant flow rate of 0.6 mL min^{-1}. HPLC data were processed with the Chromeleon 7.1.3 software (Thermo Fisher Scientific Inc.). Acetate concentrations were calculated from peak areas using calibration curves prepared with six standard concentrations ranging from 0 to 250 mM.

2.8 | Transcriptomic Analysis

Cells growing on MSM supplemented with 100 mM acetate were harvested in exponential phase at $OD_{600} = 0.6$. Culture samples of 1.5 mL were centrifuged at 12,000 × *g* for 2 min. Supernatants were removed, and RNA was isolated from cell pellets using the GeneJET RNA Purification Kit according to the manufacturer's instructions (Thermo Fisher Scientific Inc.). RNA quality and concentration were determined using a Qubit RNA High Sensitivity Assay Kit on a Qubit fluorometer (Thermo Fisher Scientific Inc.). Three biological replicates were processed per condition.

For RNA-Seq library generation and sequencing, ribosomal RNA was depleted from 100 ng total RNA using QIAseq FastSelect 5S/16S/23S, rRNA Plant, rRNA Yeast, and custom rRNA Algae depletion kits (Qiagen NV, Hilden, Germany). Libraries were prepared using the TruSeq Stranded mRNA kit (Illumina Inc.). Heat-fragmented RNA fragments of 300–400 bp were reverse-transcribed into first-strand cDNA using random hexamers and SuperScript II Reverse Transcriptase (Thermo Fisher Scientific Inc.), followed by second-strand synthesis. Double-stranded cDNA fragments were processed by A-tailing, ligated to NEXTFLEX UDI barcodes (PerkinElmer Inc., Waltham, MA, USA), and enriched using 10 cycles of PCR. Prepared libraries were quantified using the KAPA Biosystems next-generation sequencing library qPCR kit (Roche AG, Basel, Switzerland) on a LightCycler 480 real-time PCR instrument (Roche AG). Sequencing was performed on an Illumina NovaSeq instrument using NovaSeq XP v1.5 reagent kits and an S4 flow cell with a 2 × 151 indexed run configuration.

The raw FASTQ reads were filtered and trimmed using the JGI QC pipeline, yielding filtered FASTQ files. BBDuk was used to identify artefact sequences by k-mer matching with $k = 25$, allowing one mismatch, and detected artefacts were trimmed from the 3′ end of reads. RNA spike-in reads, PhiX reads and reads containing ambiguous bases were removed. Quality trimming was performed using the Phred trimming method set at Q6. After trimming, reads below the length threshold were removed. The minimum length threshold was set to 25 bp or one third of the original read length, whichever was longer. Filtered reads from each library were aligned to the reference genome using HISAT2 v2.2.1 with the −k 1 flag (Kim et al. 2015). Strand-specific coverage bigWig files were generated using deepTools v3.1 (Ramírez et al. 2014). Raw gene counts were generated from gff3 annotations using featureCounts (Liao et al. 2014). Only primary hits assigned to the reverse strand were included in raw gene counts using the −s 2, −p and -primary options. Raw gene counts were used to evaluate correlations among biological replicates using Pearson correlation and to determine which replicates were retained for differential gene expression analysis.

DESeq2 v1.30.0 (Love et al. 2014) was used to identify differentially expressed genes between pairs of conditions. Genes with adjusted *p*-values < 0.05 were considered differentially expressed (Turlin et al. 2023). A complete list of differentially expressed genes is provided in Data S1 and at the JGI Genome Portal under Project ID 1445921.

2.9 | Proteomic Analysis

P. putida SEM1.4 and derivative strains detailed in the text were precultured overnight in MSM supplemented with 20 mM acetate. Experimental cultures were performed in shaken flasks containing MSM containing 5 g L^{-1} MOPS and supplemented with 100 mM acetate and inoculated at an initial OD_{600} of 0.1. Four biological replicates were collected in mid-exponential phase at OD_{600}~1. Cells were harvested by centrifugation at

17517915, 2026, 10, Downloaded from https://environmicro-journals.onlinelibrary.wiley.com/doi/10.1111/1751-7915.70459 by Universitatsbibliothek RWTH Aachen University, Wiley Online Library on [13/11/2026]. See the Terms and Conditions (https://onlinelibrary.wiley.com/terms-and-conditions) on Wiley Online Library for rules of use; OA articles are governed by the applicable Creative Commons License

10,000 × *g* for 5 min at 4°C. Supernatants were removed, and cell pellets were frozen at −80°C until further processing.

Protein extraction from cell pellets and tryptic peptide preparation followed an established proteomic sample preparation protocol. Cell pellets were resuspended in Qiagen P2 lysis buffer (Qiagen NV). Proteins were precipitated by addition of 1 mM NaCl and four volumes of acetone, followed by two washes with 80% (*v*/*v*) acetone in water. The recovered protein pellet was homogenised in 100 mM ammonium bicarbonate in 20% (*v*/*v*) methanol. Protein concentration was determined using the DC Protein Assay (Bio-Rad Laboratories Ltd.). Proteins were reduced with 5 mM *tris*(2-carboxyethyl)phosphine for 30 min and alkylated with 10 mM iodoacetamide for 30 min at room temperature in the dark. Proteins were digested overnight with trypsin at a 1:50 trypsin-to-total protein ratio.

Peptide samples were analysed on an Agilent 1290 ultra-high-performance liquid chromatography system (Agilent Technologies Inc., Santa Clara, CA, USA) coupled to an Orbitrap Exploris 480 mass spectrometer (Thermo Fisher Scientific Inc.). Peptides were loaded onto an Ascentis ES-C18 column (Sigma-Aldrich Co., St. Louis, MO, USA) and eluted using a 10-min gradient from 98% solvent A and 2% solvent B to 65% solvent A and 35% solvent B. Solvent A was 0.1% (*v*/*v*) formic acid in water, and solvent B was 0.1% (*v*/*v*) formic acid in acetonitrile (CH_3CN). Eluting peptides were introduced into the mass spectrometer operating in positive-ion mode and analysed by data-independent acquisition. The acquisition method used a duty cycle of three survey scans from $m/z = 380$ to $m/z = 985$ and 45 MS2 scans with a precursor isolation width of 13.5 m/z to cover the mass range. DIA raw data files were analysed with DIA-NN.

The database used for DIA-NN analysis in library-free mode consisted of the latest *P. putida* KT2440 UniProt proteome FASTA sequences (Kozaeva et al. 2021) plus common proteomic contaminants. DIA-NN automatically determined mass tolerances based on first-pass analysis of the samples and optimised mass accuracy. Retention time extraction windows were determined individually for each MS run using the automated optimisation procedure implemented in DIA-NN. Protein inference was enabled, and the quantification strategy was set to Robust LC = High Accuracy. DIA-NN reports were filtered using a global false discovery rate of 0.01 at both precursor and protein-group levels.

Protein abundance was estimated using the Top3 approach, which calculates the average MS signal intensity of the three most abundant tryptic peptides detected for each protein (Silva et al. 2006; Ahrné et al. 2011; Gurdo et al. 2023). Proteomics data were analysed using a customised R script in RStudio v1.3.1093. Only proteins detected in all samples were retained. Abundance values were normalised by quantile normalisation using the R package qsmooth. Statistical differences between groups were assessed using Student's *t*-test. Data were $\log_2$-transformed for fold-change comparisons, and volcano plots were generated using VolcaNoseR (Goedhart and Luijsterburg 2020). Proteins with an absolute $\log_2$(fold change) > +1.5 and $-\log_{10}$(adjusted *p*-value) > 1.3 were considered differentially abundant.

2.10 | Fluxomic Analysis

Precultures were inoculated from freshly plated colonies of *P. putida* SEM1.4, SEM1.4^{Evo}, and SEM1.4 GacA^{E197K} FabB^{L77P} in MSM supplemented with 20 mM unlabelled acetate. Before inoculation of experimental cultures, cells were harvested by centrifugation at 10,000 × *g* for 5 min and washed twice with MSM without a carbon source. Cells were then inoculated individually at an initial $OD_{600} = 0.02$ in 100-mL shaken flasks containing 20 mL of MSM containing 5 g L^{-1} MOPS and supplemented with 100 mM labelled acetate. The labelling experiments used 99% [1-^{13}C]-sodium acetate, 99% [2-^{13}C]-sodium acetate, or 50% [U-$^{13}C_2$]-sodium acetate. The inoculum carried into labelled cultures was kept below 1% (*v*/*v*) of the final sampled biomass concentration to minimise interference from unlabelled biomass in subsequent flux calculations (Nikel et al. 2009). All experiments were performed with three biological replicates and two technical replicates. Samples were harvested during exponential growth for analysis of proteinogenic amino acids and cellular sugars. Samples were centrifuged at 10,000 × *g* for 5 min, supernatants were removed and pellets were frozen at −80°C until further processing. Cell pellets were thawed on ice and resuspended in 200 μL of 6 M HCl. Samples were incubated at 105°C for 16–24 h to hydrolyse biomass (Zamboni et al. 2009). Hydrolysed samples were filtered using a 96-well filter plate (MultiScreenHTS HV Filter Plate, 0.45 μm, hydrophilic, clear, non-sterile, EMD Millipore Corp., Burlington, MA, USA) by centrifugation at 1500 × *g* for 2 min. Filtered samples were freeze-dried and stored at −80°C. Dried samples were derivatized in two steps. First, hydrolysates were resuspended in 50 μL dimethylformamide. Second, this solution was transferred into glass vials containing 50 μL *N*-*tert*-butyldimethylsilyl-*N*-methyltrifluoroacetamide with 1% (*w*/*w*) *tert*-butyldimethylchlorosilane and incubated at 85°C for 1 h. Derivatized samples were aliquoted into glass vials with inserts for GC–MS analysis within 12 h of derivatisation.

Samples were injected into an Agilent 7890A GC–MS system (Agilent Technologies Inc.) equipped with an Agilent HP-5 ms capillary column with a length of 30 m, inner diameter of 0.25 mm and film thickness of 0.25 μm. Samples were measured in full-scan mode using the following temperature program: 120°C for 1 min, ramp to 160°C at 4°C min^{-1} and hold for 5 min, ramp to 270°C at 4°C min^{-1} and hold for 3 min, ramp to 310°C at 20°C min^{-1} and hold for 1 min, and ramp to 120°C at 60°C min^{-1}.

For analysis of cellular sugar monomers, glucose and glucosamine, cell pellets were hydrolyzed in 250 μL of 2 M HCl for 2 h at 100°C (Kiefer et al. 2004). Cell debris was removed by filtration using a 96-well filter plate. Hydrolysates were freeze-dried and stored at −80°C. Dried residues were derivatized with 2% (*w*/*v*) methoxylamine in pyridine at 80°C (1 h) and silylated with *N*,*O*-*bis*(trimethylsilyl)trifluoroacetamide (Macherey-Nagel GmbH & Co., Düren, Germany) at 80°C (30 min). Derivatized analytes were quantified on an Agilent 7890A GC–MS system (Agilent Technologies Inc.) equipped with an HP-5 ms capillary column. Samples were measured in full-scan mode using a temperature program from 120°C to 300°C. Raw chromatographic data from amino acid and sugar analyses were integrated using SmartPeak (Kutuzova et al. 2020) and corrected for natural isotope abundance in derivatization agents using INCA

17517915, 2026, 10, Downloaded from https://environmicro-journals.onlinelibrary.wiley.com/doi/10.1111/1751-7915.70459 by Universitatsbibliothek RWTH Aachen University, Wiley Online Library on [13/11/2026]. See the Terms and Conditions (https://onlinelibrary.wiley.com/terms-and-conditions) on Wiley Online Library for rules of use; OA articles are governed by the applicable Creative Commons License

(Young 2014). Mass isotopomer distributions from 14 proteinogenic amino acids were used for flux estimation, excluding cysteine and tryptophan because they degrade during hydrolysis (Nikel et al. 2015, 2021). Glutamate and aspartate were also used as proxies for glutamine and asparagine, respectively, due to deamination during protein hydrolysis. For sugar analysis, glucose fragments at $m/z = 319$ and 554 and glucosamine fragments at $m/z = 319$ and 553 were included as described by Kohlstedt and Wittmann (2019).

The acetate-dependent metabolic network for *P. putida* SEM1.4 was built from the genome-scale model *i*JN1462 (Nogales et al. 2020) with the modifications indicated by Bujdoš et al. (2023). The reconstruction included 72 reactions from central carbon metabolism; a list of reactions and the cognate carbon atom transitions are provided in Table S4. Transitions in the PP pathway (mediated by Tkt and Tal) were explicitly accounted for in the model. Fluxes were estimated with INCA using specific growth rates and acetate uptake or secretion rates as constraints, and the biomass equation was taken from Czajka et al. (2022). Relative intracellular fluxes were inferred by minimising the weighted sum of squared residuals between simulated and experimental labelling data. Flux estimation was repeated at least 20 times with random initial values until convergence. Goodness of fit was assessed using a χ^2 test, and 95% confidence intervals were calculated from the sensitivity of the residuals to flux-parameter variation (Antoniewicz et al. 2006). Flux distributions were visualised by mapping computed values onto custom metabolic maps using the R package fluctuator.

2.11 | STRING Interaction Network Analysis and Enrichment Analysis

Interaction networks for differentially regulated transcripts and proteins were obtained using the STRING v12.0 database (Szklarczyk et al. 2023). The input lists contained genes or proteins identified as differentially regulated or differentially abundant, submitted by gene names or UniProt identifiers (Pardo et al. 2022). A default confidence score threshold of 0.4, corresponding to medium confidence, was used to filter interactions. Interaction networks were visualised and clustered according to functional association (Martino et al. 2025). Networks were further analysed to identify highly connected genes or proteins and biological pathways enriched in each dataset.

2.12 | AlphaFold Prediction and Structural Characterisation

The three-dimensional structure of GacA was predicted with AlphaFold 2.0 using default settings (Jumper et al. 2021). The five highest-ranking predictions were analysed and validated using the local distance difference test, SPServer (Aguirre-Plans et al. 2021), and ProSA-Web (Wiederstein and Sippl 2007). Visualisation, structural superimposition, and in silico mutagenesis were performed with PyMOL v2.3.4 (Schrödinger Inc., New York, NY, USA). Original protein sequences were obtained from the *Pseudomonas* Database (Winsor et al. 2016). Homologue searches and sequence analyses were performed using the AlphaFold template-search algorithm, NCBI BLASTP, InterPro (Paysan-Lafosse et al. 2023), and Jalview v2.11 (Waterhouse et al. 2018).

2.13 | Data and Statistical Analysis

All experiments reported were independently repeated at least three times, and the mean values of the corresponding parameters ± standard deviations are presented. In some cases, statistical significance between groups was assessed using an unpaired Student's *t*-test. Data S1 contains the RNA-Seq, proteomic and fluxomic datasets, with titles and descriptions identifying each analysis and strain comparison. Transcript-protein agreement was assessed separately for each strain comparison by matching the corresponding gene and protein entries and calculating Spearman correlation coefficients (ρ) between their $\log_2$(fold change) values. Correlations included all matched pairs. Differential responses were classified using $|\log_2(\text{fold change})| > +1.5$ and adjusted-$p < 0.05$ in each dataset, and concordance was evaluated from the direction of change of the corresponding parameter. Data analysis was performed with MS Excel (Microsoft Corp., Redmond, WA, USA) and Prism 8 (GraphPad Software Inc., San Diego, CA, USA) unless otherwise specified.

3 | Results and Discussion

3.1 | ALE Enhances Acetate Tolerance in *P. putida*

P. putida can use a broad range of carbon substrates (Weimer et al. 2020), including acetate, a weak C_2 organic acid that becomes inhibitory at high concentrations (Kirkpatrick et al. 2001). Acetic acid (CH_3COOH), the protonated form, can diffuse across the cell envelope and dissociate in the cytosol, perturbing pH homeostasis, increasing energetic burden and triggering pleiotropic physiological damage (Trček et al. 2015; Guan and Liu 2020). Acetate tolerance is therefore expected to depend on coordinated responses across transport, central metabolism, redox balancing, membrane physiology and stress-response systems, as reported for other Gram-negative bacteria (Fernández-Sandoval et al. 2012; Rajaraman et al. 2016; Hua et al. 2024).

To investigate the mechanisms underlying acetate tolerance, we implemented an ALE strategy. Strain SEM1.4, a genome-reduced strain (Kozaeva et al. 2021; Ackermann et al. 2024) derived from *P. putida* EM42 (Martínez-García et al. 2014), was evolved in MSM under gradually increasing acetate concentrations, from 20 to 180 mM. Cultures were transferred once they reached mid-exponential phase, which under these conditions corresponds to an OD_{600}~0.5. Transfers occurred before acetate depletion, when the culture pH remained around neutrality. At the initial pH = 7.0, acetate was predominantly present in its dissociated form (CH_3COO^-), and the ALE regime selected for improved growth at elevated total acetate concentrations under initially close-to-neutral pH conditions. The selection regime therefore exposed cells to increasing acetate concentrations while limiting the alkalinisation effect associated with later cultivation stages. During the initial ALE steps, from 20 to 80 mM acetate, transfers occurred every 6–12 h. At higher concentrations, transfers were

17517915, 2026, 10, Downloaded from https://environmicro-journals.onlinelibrary.wiley.com/doi/10.1111/1751-7915.70459 by Universitatsbibliothek RWTH Aachen University, Wiley Online Library on [13/11/2026]. See the Terms and Conditions (https://onlinelibrary.wiley.com/terms-and-conditions) on Wiley Online Library for rules of use; OA articles are governed by the applicable Creative Commons License

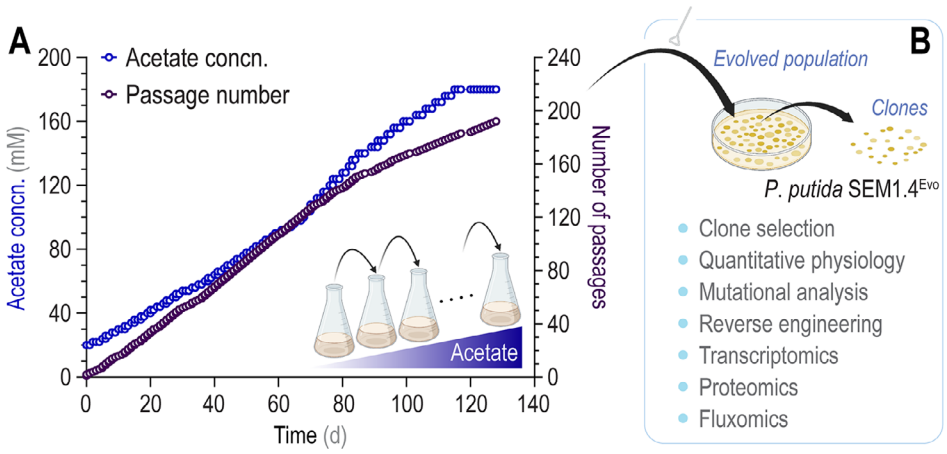


FIGURE 1 | Workflow for overcoming acetate toxicity in *P. putida* SEM1.4. (A) Adaptive laboratory evolution (ALE) strategy to increase tolerance to high acetate concentrations (concn.). (B) Physiological, mutational and multi-omic characterisation of selected evolved clones, leading to the isolation of *P. putida* SEM1.4^{Evo} for further analysis of acetate tolerance.

performed daily or after more than 24 h, as the time required to reach the target OD_{600} was increasingly longer. The evolution experiment lasted 130 days, corresponding to ca. 200 passages, and was terminated when no further growth improvement was observed after a 12-day incubation in the presence of 180 mM acetate. Under this final condition, cultures reached only OD_{600} values of ca. 0.5–0.6.

The final populations from the three ALE lineages were plated separately on MSM agar containing 180 mM acetate. Ten clones were isolated for characterisation (Figure 1A), comprising four from lineage 1 and three each from lineages 2 and 3. These clones were phenotypically characterised under increasing acetate concentrations. Whole-genome sequencing was used to identify mutations that arose during evolution, and selected mutations were introduced into the parental background by reverse engineering. The resulting strains were analysed using transcriptomics, proteomics and ^{13}C-metabolic flux analysis in an attempt to connect genotype, physiology and systems-level responses to acetate stress (Figure 1B).

3.2 | Growth Profiling of Acetate-Evolved Clones Reveals Improved Performance Under High Acetate Concentrations

The ten isolated clones and the parental strain *P. putida* SEM1.4 were challenged with increasing acetate concentrations in buffered MSM. Growth was monitored for 48 h in medium containing 20, 60, 100, 140, or 180 mM acetate. At 20 mM acetate, the parental strain and evolved clones displayed similar growth profiles, although most evolved clones reached higher final OD_{600} values after ca. 10 h of cultivation (Figure 2A). Differences became more pronounced as acetate concentration increased. At 60 and 100 mM acetate, most evolved clones displayed shorter lag phases than the parental strain, with reductions of ca. 25% and 50%, respectively (Figure 2B,C).

At 140 mM acetate, the parental strain did not show measurable growth after 48 h, whereas the evolved clones reached final OD_{600} values of ca. 2.5 (Figure 2D). This phenotype indicates that ALE substantially increased the ability of *P. putida* SEM1.4 to initiate and sustain growth under acetate concentrations that strongly inhibit the parental background. At 180 mM acetate, no detectable biomass formation was observed for either the parental strain or the evolved clones, indicating that this concentration exceeded the tolerance range achieved under the conditions used here. Overall, growth profiling showed that acetate-driven evolution mainly reduced lag phase and extended the concentration range in which *P. putida* SEM1.4 could grow, rather than enabling growth at the highest acetate concentration imposed during the evolution experiment. This phenomenon has also been observed in *P. putida* KT2440 evolved for tolerance to *p*-coumaric acid (Mohamed et al. 2020).

3.3 | Mutational Analysis Identifies Recurrent Mutations in Global Regulatory and Fatty Acid Metabolism Genes

To identify mutations associated with acetate tolerance, the ten selected clones isolated from the three evolved populations were analysed by whole-genome sequencing. The analysis focused on mutations located within coding sequences and present in most clones. Four recurrent nonsynonymous mutations were identified in genes associated with regulatory control, fatty acid biosynthesis and nucleoid organisation: *gacA* (*PP_4099*, also known as *uvrY*), encoding the response regulator of the GacS/GacA two-component system (also known as the BarA/UvrY two-component system); *fabB* (*PP_4175*), encoding a 3-oxoacyl-ACP (acyl-carrier-protein) synthase; *PP_0371*, encoding a LysR-family transcriptional regulator; and *hupB* (*PP_2303*), encoding the β subunit of a DNA-binding regulatory protein (Table 1).All ten clones carried mutations in *gacA* and *PP_0371*, nine clones carried a mutation in *fabB*, and six clones carried the *hupB*^{A35V} mutation (Table 1). Additional *hupB* and *fabB* variants appeared in single clones, suggesting lower prevalence within the evolved population. The high recurrence of the *gacA*^{E197K}, *PP_0371*^{R277H} and *fabB*^{L77P} mutations indicates strong selection for changes affecting global regulation and membrane-associated properties during growth under acetate stress.

17517915, 2026, 10, Downloaded from https://environmicro-journals.onlinelibrary.wiley.com/doi/10.1111/1751-7915.70459 by Universitatsbibliothek RWTH Aachen University, Wiley Online Library on [13/11/2026]. See the Terms and Conditions (https://onlinelibrary.wiley.com/terms-and-conditions) on Wiley Online Library for rules of use; OA articles are governed by the applicable Creative Commons License

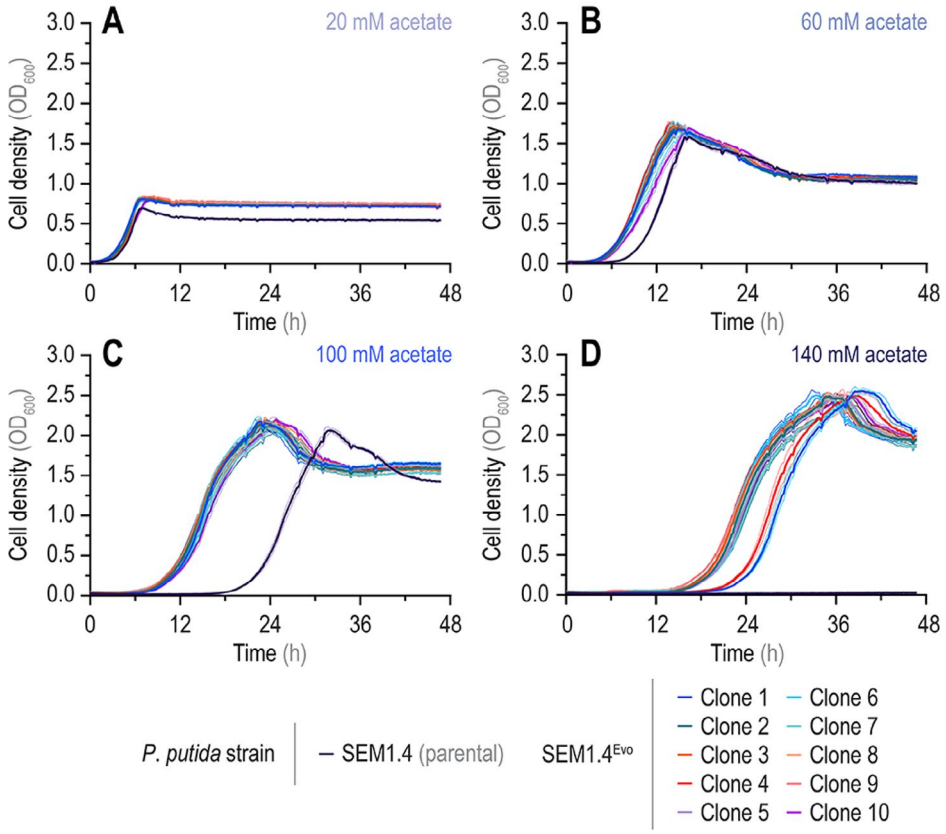


FIGURE 2 | Acetate tolerance of selected evolved clones and the parental *P. putida* strain in 96-well microtiter plates. Growth profiles of ten clones and the parental SEM1.4 strain in minimal salt medium (MSM) containing 5 g L^{-1} MOPS and supplemented with acetate at (A) 20 mM, (B) 60 mM, (C) 100 mM and (D) 140 mM. Solid lines represent mean optical density at 600 nm (OD_{600}), and shaded areas indicate the standard deviation from four biological replicates.

The GacS/GacA two-component system controls broad adaptive programs in pseudomonads, including central carbon metabolism, secondary metabolism, quorum sensing, motility and biofilm formation (Hassan et al. 2010; Song et al. 2023). Disruption of *gacA* has also been linked to improved fitness and bioproduction phenotypes in other *P. putida* backgrounds (Eng et al. 2021). The recurrence of *gacA* mutations in all acetate-evolved clones therefore points to attenuation of this regulatory system as a potential route to acetate tolerance. Consistent with this observation, mutations affecting both *gacS* and *gacA* were independently identified during acetate-driven ALE of *P. putida* KT2440, and deletion of either gene improved growth on acetate (Filbig et al. 2026). In parallel, the repeated *fabB* mutation suggests that lipid metabolism also contributed to adaptation. FabB catalyses a key elongation step in fatty acid biosynthesis and contributes to membrane composition, fluidity and integrity in *Pseudomonas* species (Hoang and Schweizer 1997; Kim et al. 2019; Yadrykhins'ky et al. 2021). Mutations in *hupB* and *PP_0371* further suggest that acetate tolerance involved broader regulatory and nucleoid-associated changes. Overall, the mutational spectrum indicates that acetate tolerance in *P. putida* SEM1.4 is a multifactorial trait shaped by coordinated changes in global regulation, fatty acid metabolism and genome-associated transcriptional control.

Interestingly, mutations affecting the GacS/GacA two-component system, including loss-of-function variants, are a common outcome of ALE in *P. putida* KT2440. The identification of the $gacA^{E197K}$ variant under acetate selection is consistent with this broader pattern of regulatory adaptation. Reverse engineering demonstrated a benefit during growth at elevated acetate concentrations, although our experiments cannot establish whether this benefit is specific to acetate or extends to other substrates. Mohamed et al. (2020) reported *gacS* mutations in all tolerance-ALE and ALE lineages evolved on hydroxycinnamates, while Bleem et al. (2024) identified *fleQ*, *gacA*/*gacS*, *wbpL* and *flgE* as the most frequently mutated loci during evolution on the lignin-derived aromatic vanillate. Convergent loss-of-function mutations in *gacA* and *gacS* were detected under ALE with terephthalate and terephthalate-ethylene glycol. Reverse engineering showed that deletion of *gacA* or *gacS* shortened lag phase and improved growth and substrate utilization (Werner et al. 2025). GacS/GacA disruption has been interpreted as a substrate-independent adaptation to well-mixed, nutrient-defined batch cultivation, where downregulation of costly flagellar, biofilm and secondary-metabolic programs redirects resources toward growth. This explanation echoes the tendency of *Pseudomonas* to accumulate spontaneous *gacS*/*gacA* mutations in laboratory cultures, first characterised in biocontrol strains where these mutations abolish secondary-metabolite production and where loss of costly secondary metabolism can drive mutant enrichment (Duffy and Défago 2000; Bull et al. 2001; van den Broek et al. 2005; Yan et al. 2018). The emergence of *gacA* mutations under acetate selection extends

17517915, 2026, 10, Downloaded from https://environmicro-journals.onlinelibrary.wiley.com/doi/10.1111/1751-7915.70459 by Universitatsbibliothek RWTH Aachen University, Wiley Online Library on [13/11/2026]. See the Terms and Conditions (https://onlinelibrary.wiley.com/terms-and-conditions) on Wiley Online Library for rules of use; OA articles are governed by the applicable Creative Commons License

TABLE 1 | Mutational analysis of selected clones after evolution in the presence of acetate.

Position (bp)	Mutation type	Sequence change	Gene name or locus ID[a]	Gene annotation[b]	Details	Clone #									
						1	2	3	4	5	6	7	8	9	10
451,043	SNP	C → T	*PP_0371*	Transcriptional regulator, LysR family	R277H (CGC → CAC)	+	+	+	+	+	+	+	+	+	+
4,635,167	SNP	C → T	*PP_4099, gacA*	Two-component system GacS/GacA, regulatory subunit	E197K (GAA → AAA)	+	+	+	+	+	+	+	+	+	+
4,717,665	SNP	T → C	*PP_4175, fabB*	3-oxoacyl-ACP synthase	L77P (CTG → CCG)	+	+	+	+	+	+	+	+	+	
2,633,188	SNP	C → T	*PP_2303, hupB*	DNA binding regulator, β subunit B	A35V (GCC → GTC)	+	+		+	+	+		+		
2,633,230	SNP	C → T	*PP_2303, hupB*	DNA binding regulator, β subunit B	T49I (ACC → ATC)									+	
2,633,326	SNP	C → T	*PP_2303, hupB*	DNA binding regulator, β subunit B	A81V (GCC → GTC)										+
4,717,483	SNP	C → T	*PP_4175, fabB*	3-oxoacyl-ACP synthase 1	G16G (GGC → GGT)										+

[a]Single nucleotide polymorphisms (SNPs) found in the isolated clones after whole-genome sequencing.
[b]Annotation according to the *Pseudomonas* Genome Database (Winsor et al. 2016).

17517915, 2026, 10, Downloaded from https://environmicro-journals.onlinelibrary.wiley.com/doi/10.1111/1751-7915.70459 by Universitatsbibliothek RWTH Aachen University, Wiley Online Library on [13/11/2026]. See the Terms and Conditions (https://onlinelibrary.wiley.com/terms-and-conditions) on Wiley Online Library for rules of use; OA articles are governed by the applicable Creative Commons License

the convergent GacS/GacA signature to non-aromatic carbon sources. Considering these results, clone 6 from lineage 1 was selected for further analysis and designated *P. putida* SEM1.4^{Evo}.

3.4 | Reverse Engineering of Recurrent Mutations Links *gacA* and *fabB* Variants to Acetate Tolerance

To evaluate the contribution of recurrent ALE mutations to acetate tolerance, we introduced selected single-nucleotide substitutions into the genome of the parental strain *P. putida* SEM1.4. Mutation selection was based on prevalence across the evolved clones, using a threshold > 50% (Table 1). This criterion prioritised four nonsynonymous substitutions (nucleotide changes in the corresponding gene are indicated in bold, underlined): PP_0371^{R277H} (CGC → C**A**C), GacA^{E197K} (GAA → **A**AA), FabB^{L77P} (CTG → C**C**G) and HupB^{A35V} (GCC → G**T**C). The corresponding single mutants were constructed by scarless allelic exchange, and their growth was evaluated under increasing acetate concentrations (Figure 3).

At 20 mM acetate, all strains displayed comparable growth profiles (Figure 3A). Differences became evident at higher substrate concentrations. Strains carrying the *gacA*^{E197K}, *fabB*^{L77P}, or *hupB*^{A35V} alleles showed shorter lag phases than the parental strain, particularly above 60 mM acetate (Figure 3B–E and Table 2). The strongest single-mutation effects were observed for strains carrying the reverse-engineered *gacA*^{E197K} and *fabB*^{L77P} variants. In contrast, strain PP_0371^{R277H} showed impaired growth across the tested conditions and was not pursued further. The parental strain expectedly failed to grow at 120–140 mM acetate even after a 72-h incubation, whereas several reverse-engineered strains retained measurable growth at 120 mM acetate (Figure 3F).Because the strains individually carrying the *gacA*^{E197K} and *fabB*^{L77P} alleles had the clearest improvements among the single mutants, we combined both mutations (*P. putida* SEM1.4 GacA^{E197K} FabB^{L77P}) to examine whether they jointly reproduced the evolved phenotype. The double mutant closely matched strain SEM1.4^{Evo} across most acetate concentrations, with a markedly reduced lag phase and sustained growth at substrate concentrations that inhibited the parental strain (Figure 3 and Table 2). Importantly, unlike the other reverse-engineered strains, the GacA^{E197K} FabB^{L77P} strain grew at 140 mM acetate (Figure 3G). These results indicate that the *gacA*^{E197K} and *fabB*^{L77P} mutations recapitulate much of the acetate-tolerant phenotype obtained through ALE, although additional mutational effects may contribute to the behaviour of the evolved clone.

Since the GacS/A system mediates global regulation in pseudomonads, we analysed the GacA mutation in silico at the structural level. The GacA^{E197K} substitution mapped to the C-terminal LuxR/FixJ-type helix-turn-helix domain (Figure S1), associated with DNA recognition and transcriptional regulation (Kahn and Ditta 1991; Sitnikov et al. 1995). Structural modelling suggested that the charge reversal could alter the local environment around residue 197 (Figure S1A,B). These predictions are compatible with impaired GacA activity, although altered DNA binding or loss of function cannot be established. Based on these results, we continued our analysis of acetate tolerance with quantitative physiology experiments.

3.5 | Physiological Characterisation of the Reverse-Engineered Double Mutant Substantiates the Evolved Phenotype and Connects Acetate Tolerance to Resource-Efficient Carbon Use

To evaluate whether the reverse-engineered mutations reproduced the evolved phenotype under standard shaken-flask conditions, we characterised *P. putida* SEM1.4, strain SEM1.4^{Evo}, and the double mutant strain GacA^{E197K} FabB^{L77P} in MSM

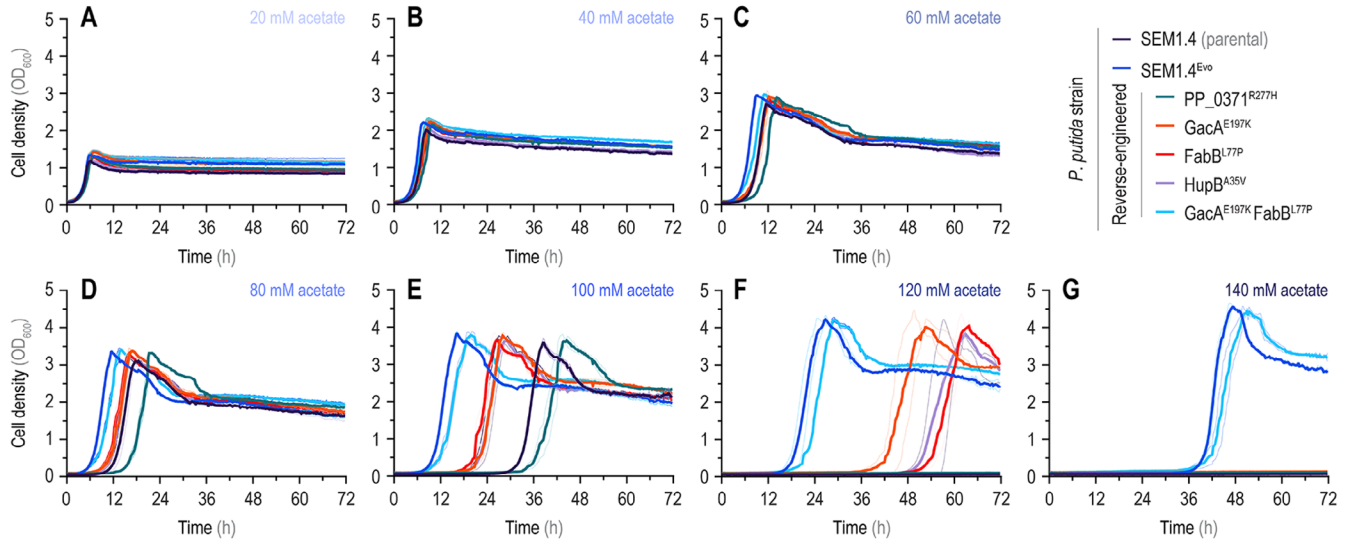


FIGURE 3 | Evaluation of parental, evolved and reverse-engineered strains carrying key single-nucleotide polymorphisms (SNPs) at low, medium and high acetate concentrations. The reverse-engineered strains carrying the PP_0371^{R277H}, GacA^{E197K}, FabB^{L77P}, HupB^{A35V} and GacA^{E197K} FabB^{L77P} modifications were tested in minimal salt medium (MSM) containing 5 g L^{-1} MOPS and supplemented with acetate at (A) 20 mM, (B) 40 mM, (C) 60 mM, (D) 80 mM, (E) 100 mM, (F) 120 mM and (G) 140 mM, and compared to the parental *P. putida* SEM1.4 strain and its evolved derivative (SEM1.4^{Evo}). Solid lines represent mean values, and shaded areas indicate the standard deviation from four biological replicates.

17517915, 2026, 10, Downloaded from https://environmicro-journals.onlinelibrary.wiley.com/doi/10.1111/1751-7915.70459 by Universitatsbibliothek RWTH Aachen University, Wiley Online Library on [13/11/2026]. See the Terms and Conditions (https://onlinelibrary.wiley.com/terms-and-conditions) on Wiley Online Library for rules of use; OA articles are governed by the applicable Creative Commons License

TABLE 2 | Growth parameters[a] of *P. putida* SEM1.4, SEM1.4^{Evo} and reverse-engineered strains grown with increasing acetate concentrations.

Acetate concentration (mM)	SEM1.4	SEM1.4^{Evo}	PP0371^{R277H}	GacA^{E197K}	FabB^{L77P}	HupB^{A35V}	GacA^{E197K} FabB^{L77P}
Specific growth rate (μ, h^{-1}) for strain							
20	0.78 ± 0.03	0.75 ± 0.02	0.72 ± 0.02	0.72 ± 0.02	0.73 ± 0.01	0.73 ± 0.02	0.69 ± 0.02
40	0.73 ± 0.01	0.67 ± 0.03	0.68 ± 0.01	0.63 ± 0.01	0.64 ± 0.02	0.64 ± 0.01	0.59 ± 0.03
60	0.62 ± 0.01	0.66 ± 0.03	0.62 ± 0.01	0.57 ± 0.01	0.61 ± 0.02	0.58 ± 0.01	0.54 ± 0.01
80	0.58 ± 0.01	0.59 ± 0.01	0.59 ± 0.01	0.53 ± 0.02	0.55 ± 0.01	0.53 ± 0.01	0.51 ± 0.02
100	0.52 ± 0.01	0.54 ± 0.01	0.52 ± 0.01	0.49 ± 0.02	0.51 ± 0.01	0.51 ± 0.01	0.47 ± 0.02
120	N.G.	0.53 ± 0.02	N.G.	0.44 ± 0.01	0.43 ± 0.05	0.38 ± 0.11	0.45 ± 0.02
140	N.G.	0.49 ± 0.01	N.G.	N.G.	N.G.	N.G.	0.42 ± 0.01
Lag phase (λ, h)							
20	1.7 ± 0.2	1.6 ± 0.1	1.9 ± 0.1	1.8 ± 0.1	1.7 ± 0.2	1.7 ± 0.1	1.4 ± 0.1
40	2.5 ± 0.1	1.4 ± 0.1	2.9 ± 0.1	2.2 ± 0.3	1.9 ± 0.3	2.3 ± 0.3	1.6 ± 0.1
60	4.3 ± 0.1	2.2 ± 0.1	5.5 ± 0.1	3.7 ± 0.4	3.2 ± 0.3	4.0 ± 0.1	2.2 ± 0.2
80	8.9 ± 0.6	3.1 ± 0.1	11.3 ± 0.2	6.3 ± 0.5	5.4 ± 0.5	7.5 ± 0.1	3.3 ± 0.1
100	26.7 ± 2.6	6.2 ± 0.3	29.1 ± 0.8	15.8 ± 0.6	13.6 ± 0.9	19.2 ± 0.6	6.6 ± 0.4
120	N.G.	14.8 ± 1.1	N.G.	36.8 ± 5.7	40.3 ± 4.1	63.4 ± 3.2	15.1 ± 0.2
140	N.G.	33.3 ± 4.1	N.G.	N.G.	N.G.	N.G.	32.2 ± 1.3

Abbreviation: N.G., no growth.
[a]Cells were grown in minimal salt medium (MSM) containing 5 g L^{-1} MOPS and supplemented with the indicated acetate concentrations in 96-well microtiter plates. In all cases, results represent mean values ± standard deviation from at least four independent experiments.

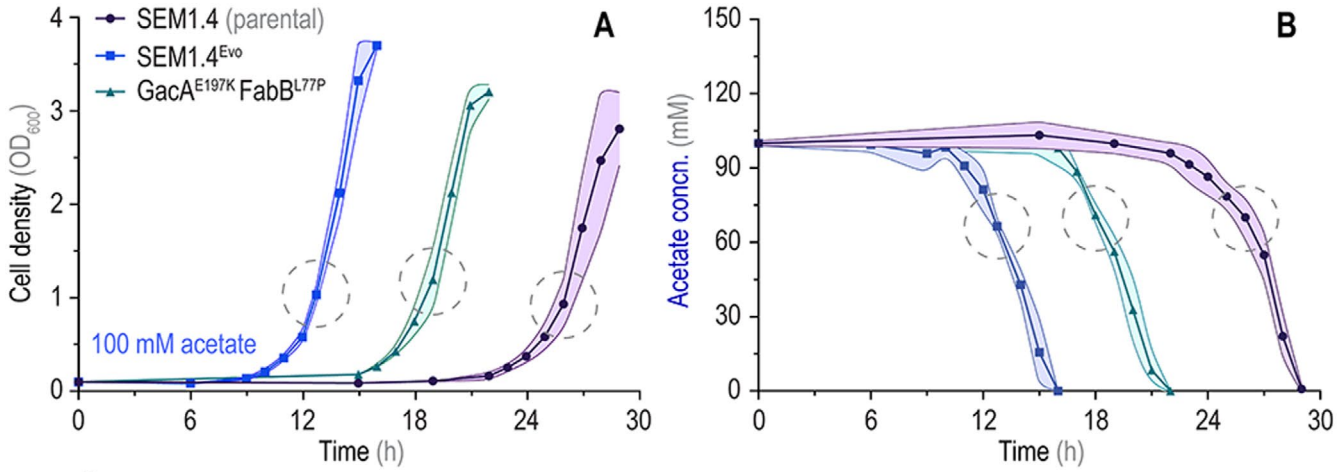
containing 5 g L^{-1} MOPS and supplemented with 100 mM acetate. This concentration was selected because it was the lowest acetate level that differentiated the strains during microplate screening (Figure 3E). Samples for transcriptomic and proteomic analyses were collected during mid-exponential growth. At the corresponding sampling points, ca. 40 mM acetate had been consumed and the culture pH ranged from 7.6 to 7.8. Further alkalinisation occurred toward the end of cultivation, when most of the acetate had been depleted, and the medium reached pH > 8.5. In this sense, the physiological measurements represent different extracellular conditions over the course of cultivation. Endpoint biomass measurements could also reflect late-stage alkalinisation effects, whereas the transcriptomic and proteomic profiles described cells sampled earlier, with acetate still available and the pH not substantially affected.

Shaken-flask cultivations established that acetate-driven evolution improved growth under acetate stress. The parental strain displayed a lag phase of ca. 22 h, whereas strain SEM1.4^{Evo} and the reverse-engineered variant had shorter lag phases of ca. 9 and 15 h, respectively (Figure 4A). Acetate consumption followed the growth profiles (Figure 4B), although the parental strain had the highest specific acetate uptake rate (q_A), reaching 34.1 ± 4.7 mmol $g_{CDW}^{-1} h^{-1}$, substantially higher than 25.9 ± 0.8 mmol $g_{CDW}^{-1} h^{-1}$ for strain SEM1.4^{Evo} and 23.8 ± 1.6 mmol $g_{CDW}^{-1} h^{-1}$ for the GacA^{E197K} FabB^{L77P} strain (Figure 4C). In this context, however, faster acetate uptake by the parental strain did not lead to higher biomass formation. This phenotype indicates that acetate tolerance was not driven by faster acetate consumption alone, but by more efficient conversion of acetate carbon into biomass.

This yield phenotype is central to the mechanistic interpretation of the evolved state. Both strain SEM1.4^{Evo} and the double mutant displayed 16%–25% faster growth and had 60%–70% higher biomass yields than the parental strain (Figure 4C). Higher biomass yields indicate that a larger fraction of the consumed acetate was retained in cellular material, potentially reducing carbon losses through CO_2 release, maintenance metabolism, oxidative-stress management, or futile cycling through central metabolism. The double mutant reproduced most of this improvement in physiological parameters, linking the *gacA*^{E197K} and *fabB*^{L77P} mutations to a resource-efficient acetate-use phenotype.

These physiological differences define the basis for the multiomic analyses that follow. If the evolved and reverse-engineered strains use acetate more efficiently, their transcriptomes, proteomes, and fluxomes should reveal reduced investment in costly non-essential functions and a reorganisation of central carbon metabolism toward carbon conservation. The sections below test this model and show that the higher biomass yield is associated with global regulatory rewiring, reduced expression of energetically expensive stress and secretion programs, altered fatty acid metabolism and flux redistribution toward acetate-conserving routes.

17517915, 2026, 10, Downloaded from https://environmicro-journals.onlinelibrary.wiley.com/doi/10.1111/1751-7915.70459 by Universitatsbibliothek RWTH Aachen University, Wiley Online Library on [13/11/2026]. See the Terms and Conditions (https://onlinelibrary.wiley.com/terms-and-conditions) on Wiley Online Library for rules of use; OA articles are governed by the applicable Creative Commons License



C

P. putida strain	Specific growth rate (μ, h^{-1})	Specific rate of acetate uptake (q_A, mmol g_{CDW}^{-1} h^{-1})	Biomass yield ($Y_{X/S}$, g_{CDW} $g_{acetate}^{-1}$)
SEM1.4 (parental)	0.44 ± 0.02	34.1 ± 4.7	0.13 ± 0.02
SEM1.4^{Evo}	0.55 ± 0.01	25.9 ± 0.8	0.21 ± 0.01
GacA^{E197K} FabB^{L77P}	0.51 ± 0.03	23.8 ± 1.6	0.22 ± 0.02

FIGURE 4 | Quantitative physiological characterisation of relevant *P. putida* strains in shaken-flask cultivations. *P. putida* SEM1.4, SEM1.4^{Evo} and the reverse-engineered GacA^{E197K} FabB^{L77P} strain were grown in MSM containing 5 g L^{-1} MOPS and supplemented with 100 mM acetate to evaluate (A) growth profiles and (B) acetate consumption. Solid lines represent mean values, and shaded areas indicate the standard deviation from three biological replicates. Dotted circles indicate the sampling point for multi-omic analyses during mid-exponential growth. Specific growth rates, acetate uptake rates and biomass yields are shown in (C) as mean values ± standard deviation. CDW, cell dry weight.

3.6 | Transcriptomic Profiling Identifies Repression of Costly Cellular Programs

To identify transcriptional changes associated with acetate tolerance, RNA-Seq analysis was performed with the parental strain SEM1.4, strain SEM1.4^{Evo}, and the reverse-engineered GacA^{E197K} FabB^{L77P} strain during growth in MSM containing 5 g L^{-1} MOPS and supplemented with 100 mM acetate. Samples were collected in exponential phase, and differential gene expression was evaluated across three pairwise comparisons: strain SEM1.4^{Evo} versus the parental strain SEM1.4, the GacA^{E197K} FabB^{L77P} strain versus the parental strain SEM1.4, and the GacA^{E197K} FabB^{L77P} strain versus strain SEM1.4^{Evo} (Figure 5A–D). These comparisons were chosen to determine whether the two reverse-engineered mutations reproduced the regulatory state selected during acetate-driven evolution.

Relative to the parental strain SEM1.4, strain SEM1.4^{Evo} showed broad transcriptional remodelling, with 208 differentially expressed genes, including 27 upregulated and 181 downregulated genes (Figure 5A,D). The induced gene set included those encoding putrescine catabolism, amino acid transport, energy metabolism and transcriptional regulation. These comprised *aphA*, encoding an acetylpolyamine aminohydrolase, *potF-IV*, encoding putrescine-binding periplasmic proteins, *gabD-II*, encoding an $NADP^+$-dependent succinate-semialdehyde dehydrogenase, and *PP_1298* and *PP_1299*, the permease components of amino acid ABC transporters. The upregulation of *scpC* (encoding an acetate: succinate CoA transferase) and *sucC* and *sucD* (encoding subunits of succinyl-CoA synthetase) further points to increased use of succinyl-CoA–linked reactions and alternative routes feeding succinate metabolism (Figure S2A). This response is consistent with a shift toward acetate assimilation routes that support growth while maintaining precursor supply under stress.

The most prominent transcriptional signature in strain SEM1.4^{Evo} was gene repression. The downregulated gene fraction was dominated by secretion systems, environmental sensing, carbohydrate storage, glycosyl transferase functions and fatty acid biosynthesis. Several components of the type VI secretion system (T6SS) were repressed, including genes from the K1-T6SS and K3-T6SS clusters, orphan *hcp*-associated loci, and *vgrG*-linked clusters (Figure S2B). Given the control of T6SS expression by the Gac/Rsm regulatory cascade in pseudomonads, repression of this program is consistent with altered Gac/Rsm signalling in the adapted strains. The evolved strain also downregulated two-component regulatory genes, glycogen-, trehalose- and maltose-associated genes, and a fatty acid metabolism cluster spanning *PP_3775* to *PP_3787*. These changes hint at reduced investment in non-essential secretion functions, sensing, storage and membrane-building functions during growth on acetate.

The reverse-engineered double mutant showed a transcriptional response that largely mirrored that of the evolved strain. Relative to the parental strain SEM1.4, strain GacA^{E197K} FabB^{L77P} displayed extensive differential gene expression dominated by downregulated genes (Figure 5B,D). The few upregulated functions again included polyamine transport and catabolism, amino acid transport, iron uptake and energy metabolism, although these genes did not form a clearly resolved STRING cluster (Figure S3A), whereas downregulated functions largely overlapped with those observed in

17517915, 2026, 10, Downloaded from https://environmicro-journals.onlinelibrary.wiley.com/doi/10.1111/1751-7915.70459 by Universitatsbibliothek RWTH Aachen University, Wiley Online Library on [13/11/2026]. See the Terms and Conditions (https://onlinelibrary.wiley.com/terms-and-conditions) on Wiley Online Library for rules of use; OA articles are governed by the applicable Creative Commons License

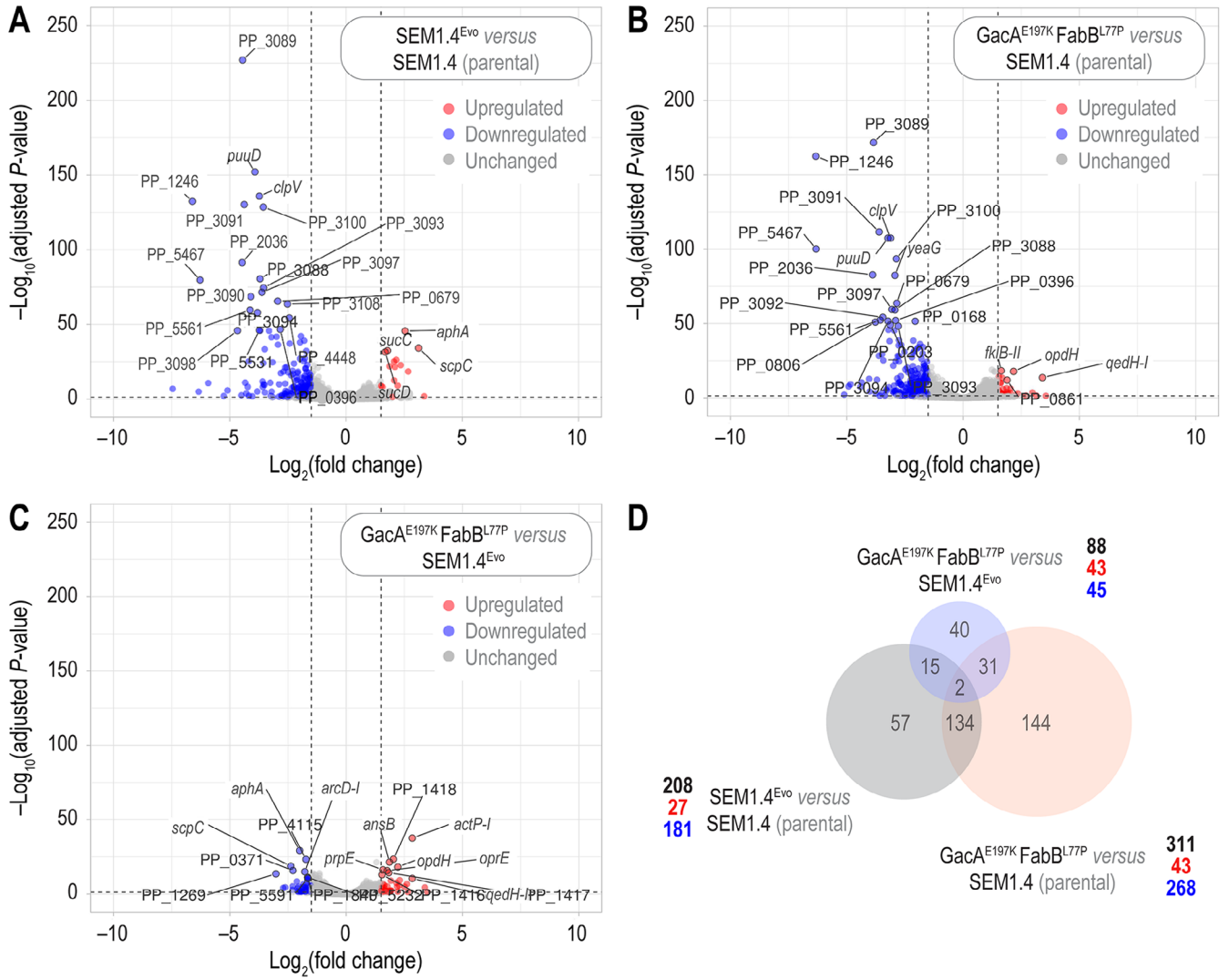


FIGURE 5 | Transcriptomic analysis. Volcano plots of RNA-Seq data showing differentially expressed transcripts in *P. putida* SEM1.4^{Evo} versus the parental strain SEM1.4 (A), the reverse-engineered GacA^{E197K} FabB^{L77P} strain versus the parental strain SEM1.4 (B), and the reverse-engineered GacA^{E197K} FabB^{L77P} strain versus *P. putida* SEM1.4^{Evo} (C). Three biological replicates were grown in MSM containing 5 g L^{-1} MOPS and supplemented with 100 mM acetate and harvested during mid-exponential growth. Horizontal and vertical dashed lines indicate the significance threshold (adjusted *p*-value < 0.05) and fold-change thresholds [|log$_2$(fold change)| > +1.5]. (D) Venn diagram illustrating the overlap of significantly differentially expressed transcripts among the three pairwise comparisons indicated in (A–C), with circle areas proportional to the total number of differentially expressed transcripts in each comparison. Numbers within the circles indicate transcripts unique to or shared among strains. Numbers adjacent to each comparison indicate the total number of differentially expressed transcripts (black), including upregulated (red) and downregulated (blue) transcripts.

strain SEM1.4^{Evo}. In particular, genes encoding T6SS, various two-component sensory systems, carbohydrate-storage functions, glycosyl transferases and fatty acid metabolism were consistently repressed in both acetate-adapted backgrounds (Figure S3B). This substantial regulatory overlap indicates that the *gacA*^{E197K} and *fabB*^{L77P} mutations were sufficient to reproduce a large fraction of the evolved transcriptional program.

Direct comparison between strain SEM1.4 GacA^{E197K} FabB^{L77P} and strain SEM1.4^{Evo} revealed a smaller set of differentially expressed genes, consistent with phenotypic convergence between the two backgrounds (Figure 5C,5D). Genes upregulated in the double mutant relative to strain SEM1.4^{Evo} included the tricarboxylate transporter genes *tctABC*, the outer membrane, tricarboxylate-specific porin *opdH*, and the acetate permease *actP-I*. These changes suggest that the double mutant may retain higher expression of transport functions linked to organic acid uptake. Conversely, genes with lower expression in the double mutant included *scpC*, heat-shock and redox-associated genes, arginine catabolism genes and nitrogen-assimilation functions. Overall, the transcriptomic data support a model in which acetate tolerance arises from *gacA*- and *fabB*-linked regulatory rewiring that reduces investment in costly stress-, secretion-, storage- and membrane-associated programs. This transcriptional economy provides a plausible route to the higher biomass yield observed in the evolved and reverse-engineered strains.

17517915, 2026, 10, Downloaded from https://environmicro-journals.onlinelibrary.wiley.com/doi/10.1111/1751-7915.70459 by Universitatsbibliothek RWTH Aachen University, Wiley Online Library on [13/11/2026]. See the Terms and Conditions (https://onlinelibrary.wiley.com/terms-and-conditions) on Wiley Online Library for rules of use; OA articles are governed by the applicable Creative Commons License

3.7 | Proteomic Remodelling Supports Reduced Stress Burden and Resource Reallocation During Acetate Adaptation

Proteome-wide changes were quantified in the parental strain SEM1.4, strain SEM1.4^{Evo}, and the reverse-engineered strain GacA^{E197K} FabB^{L77P} during exponential growth in MSM containing 5 g L^{-1} MOPS and supplemented with 100 mM acetate. Protein-abundance changes were analysed as $\log_2$(fold change) relative to the parental strain SEM1.4 or strain SEM1.4^{Evo}, and differentially abundant proteins were visualised as volcano plots (Figure 6A–C). In agreement with the transcriptome, both acetate-adapted backgrounds showed extensive proteome remodelling relative to the parental strain SEM1.4 (Figure S4A,B), whereas direct comparison between the double mutant and strain SEM1.4^{Evo} revealed only a limited set of differences (Figure 6D). This pattern further supports the notion that the two reverse-engineered mutations captured much of the evolved systems-level response.

Several proteomic changes point to altered sulphur and methionine metabolism under acetate stress. MetN1, a methionine transport ATP-binding protein, and CysZ, a sulphate permease, were strongly increased in abundance in the adapted backgrounds. In contrast, proteins linked to organosulfur utilisation and homocysteine metabolism, including SsuD, SsuF, GlpE and MetY, were reduced. Methionine metabolism has been associated with protection against acetate-induced stress in bacteria, in part through its connection to homocysteine toxicity and sulphur assimilation (Mordukhova and Pan 2013). The protein-abundance pattern observed here draws a connection between acetate adaptation and sulphur allocation and

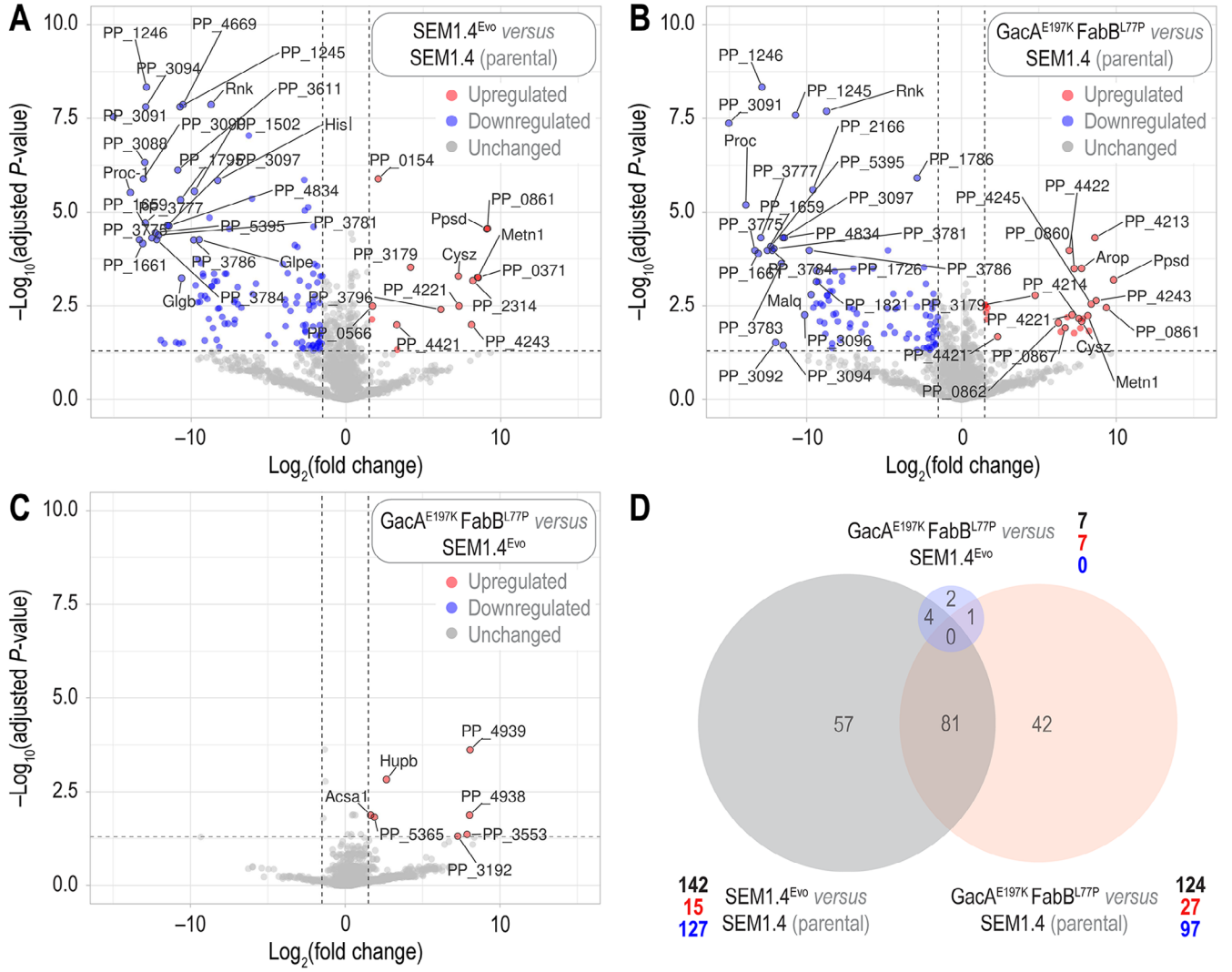


FIGURE 6 | Proteomic analysis. Volcano plots showing differentially abundant proteins in *P. putida* SEM1.4^{Evo} versus the parental strain SEM1.4 (A), the reverse-engineered GacA^{E197K} FabB^{L77P} strain versus the parental strain SEM1.4 (B), and the reverse-engineered GacA^{E197K} FabB^{L77P} strain versus *P. putida* SEM1.4^{Evo} (C). Four biological replicates were grown in MSM containing 5 g L^{-1} MOPS and supplemented with 100 mM acetate and harvested during mid-exponential growth. Horizontal and vertical dashed lines indicate the significance threshold (adjusted p-value <0.05) and fold-change thresholds [$|\log_2$(fold change)$| > +1.5$]. (D) Venn diagram illustrating the overlap of significantly differentially abundant proteins among the three pairwise comparisons indicated in (A–C), with circle areas proportional to the total number of differentially abundant proteins in each comparison. Numbers within the circles indicate proteins unique to or shared among strains. Numbers adjacent to each comparison indicate the total number of differentially abundant proteins (black), including proteins with increased (red) and decreased (blue) abundance.

17517915, 2026, 10, Downloaded from https://environmicro-journals.onlinelibrary.wiley.com/doi/10.1111/1751-7915.70459 by Universitatsbibliothek RWTH Aachen University, Wiley Online Library on [13/11/2026]. See the Terms and Conditions (https://onlinelibrary.wiley.com/terms-and-conditions) on Wiley Online Library for rules of use; OA articles are governed by the applicable Creative Commons License

methionine-associated metabolism, which potentially reduces the cost of stress management while preserving essential biosynthetic capacity.

A second major proteomic signature involved oxidative stress management. Proteins involved in reactive oxygen species detoxification, for example, glutathione *S*-transferases, thiol peroxidase, catalase-peroxidase, superoxide dismutase and cytochrome *c*-associated functions, were less abundant in strain SEM1.4^{Evo} and in the double mutant than in the parental SEM1.4 strain. The lower abundance of these proteins could indicate a reduced requirement for detoxification or altered regulation of oxidative-stress defences associated with GacA attenuation, as suggested by the transcriptional response to *gacA* inactivation in *P. fluorescens* Pf-5 (Hassan et al. 2010). The result aligns with the physiological data: the parental strain consumed acetate ca. 32% faster than SEM1.4^{Evo} but converted the substrate less efficiently into biomass, whereas evolved and reverse-engineered strains achieved substantially higher biomass yields with lower acetate uptake. Together, these observations suggest a reduced requirement for oxidative-stress compensation.

Proteomic changes also indicate remodelling of iron acquisition and fatty acid metabolism. Proteins associated with iron homeostasis and pyoverdine-linked functions were highly upregulated in the evolved and double mutant strains, consistent with the known connection between iron availability, oxidative stress, and the GacS/A regulatory network (Song et al. 2023). In parallel, proteins involved in β-oxidation and fatty acid metabolism, including FadE, several acyl-CoA dehydrogenases, and a cyclopropane-fatty-acyl-phospholipid synthase, were reduced in the acetate-adapted backgrounds. This pattern posits that acetate adaptation decreased reliance on fatty acid turnover and membrane remodelling while redirecting acetyl-CoA and energy resources toward growth-supporting metabolism. The recurrence of the *fabB*^{L77P} mutation further supports a role for lipid metabolism and membrane physiology in acetate tolerance.

Direct comparison of matched transcript and protein measurements revealed agreement in both comparisons against the parental strain. Spearman correlations between $\log_2$(fold change) values were $\rho = 0.393$ across 1788 matched pairs for strain SEM1.4^{Evo} and $\rho = 0.366$ across 1790 pairs for the GacA^{E197K} FabB^{L77P} strain. All pairs meeting the significance and effect-size thresholds in both datasets changed in the same direction, comprising 53 decreases and four increases in SEM1.4^{Evo}, and 49 decreases and two increases in the reverse-engineered strain. Concordant decreases included the T6SS-associated proteins ClpV and PP_3089/Hcp and the carbohydrate-metabolism proteins TreZ, MalQ and GlgE in both comparisons. GlgA and TreY also decreased at both levels in SEM1.4Evo. These results point to coordinated changes in selected secretion and carbohydrate storage-associated functions extending from transcription to protein abundance.

Furthermore, the combination of T6SS repression, increased abundance of pyoverdine-associated proteins, and decreased abundance of several oxidative-stress defence proteins shares features with the transcriptional response to *gacA* inactivation in *P. fluorescens* Pf-5. Hassan et al. (2010) reported decreased expression of T6SS genes, including *hcp*, and genes encoding iron-containing superoxide dismutase, catalase, and cytochrome *c* peroxidase, together with increased expression of pyoverdine biosynthesis and iron-acquisition genes. This observation evidences attenuated GacA-dependent regulation as a possible consequence of the GacA^{E197K} substitution. Since our multi-omic analyses characterised the evolved strain and the reverse-engineered double mutant, which also carried *fabB*^{L77P}, these comparisons do not resolve the individual contribution of each substitution or establish whether GacA^{E197K} caused partial or complete loss of function. Nevertheless, the proteomic data reinforce the resource-reallocation model suggested by the transcriptome. In this sense, the evolved and reverse-engineered strains showed reduced abundance of proteins linked to energetically expensive stress responses, secretion programs, lipid turnover, and oxidative-stress defence (Figure S5A,B). These changes help explain why acetate tolerance was associated with higher biomass yield rather than increased acetate uptake. In this model, the *gacA*^{E197K} and *fabB*^{L77P} mutations reprogram cellular resource allocation, reducing carbon and energy loss through stress-associated functions and improving biomass formation per acetate consumed.

3.8 | ^{13}C-Metabolic Flux Analysis Reveals Carbon-Conserving Rewiring of Acetate Metabolism

The transcriptomic and proteomic profiles suggest that acetate adaptation reduced investment in energetically costly stress-response and non-essential cellular programs. To determine whether this regulatory shift was accompanied by changes in intracellular carbon distribution, we performed network-wide ^{13}C-metabolic flux analysis during growth on 100 mM acetate (Figure 7). The parental strain SEM1.4, strain SEM1.4^{Evo} and the reverse-engineered GacA^{E197K} FabB^{L77P} strain were cultivated with parallel acetate tracers, and labelling patterns from proteinogenic amino acids and cellular sugars were used to estimate central carbon fluxes (Figure 7A).

Flux distributions differed markedly between the parental strain SEM1.4 and the two acetate-adapted backgrounds. The parental strain showed substantial flux through the pentose phosphate pathway (Figure 7B), consistent with activation of cyclic central carbon routes upon acetate supplementation. Such cycling can support redox balancing and precursor supply (Nikel et al. 2021), but it also increases carbon and energy expenditure under stress conditions. In contrast, strain SEM1.4^{Evo} and the double mutant showed strongly reduced flux through these routes, indicating that acetate adaptation attenuated non-productive metabolic cycling.

The adapted strains also redirected a larger fraction of acetate-derived carbon through carbon-conserving routes. During growth on acetate, ca. 50% of the carbon reaching the acetyl-CoA node entered the glyoxylate shunt in the parental strain SEM1.4 relative to the citrate/isocitrate branch (Figure 7B), whereas this fraction increased to ca. 60% in strain SEM1.4^{Evo} and the double mutant (Figure 7C,D). Increased glyoxylate shunt flux is consistent with improved carbon retention because this route bypasses the CO_2-generating steps of the TCA cycle and supports formation of C_4 precursors required for

17517915, 2026, 10, Downloaded from https://environmicro-journals.onlinelibrary.wiley.com/doi/10.1111/1751-7915.70459 by Universitatsbibliothek RWTH Aachen University, Wiley Online Library on [13/11/2026]. See the Terms and Conditions (https://onlinelibrary.wiley.com/terms-and-conditions) on Wiley Online Library for rules of use; OA articles are governed by the applicable Creative Commons License

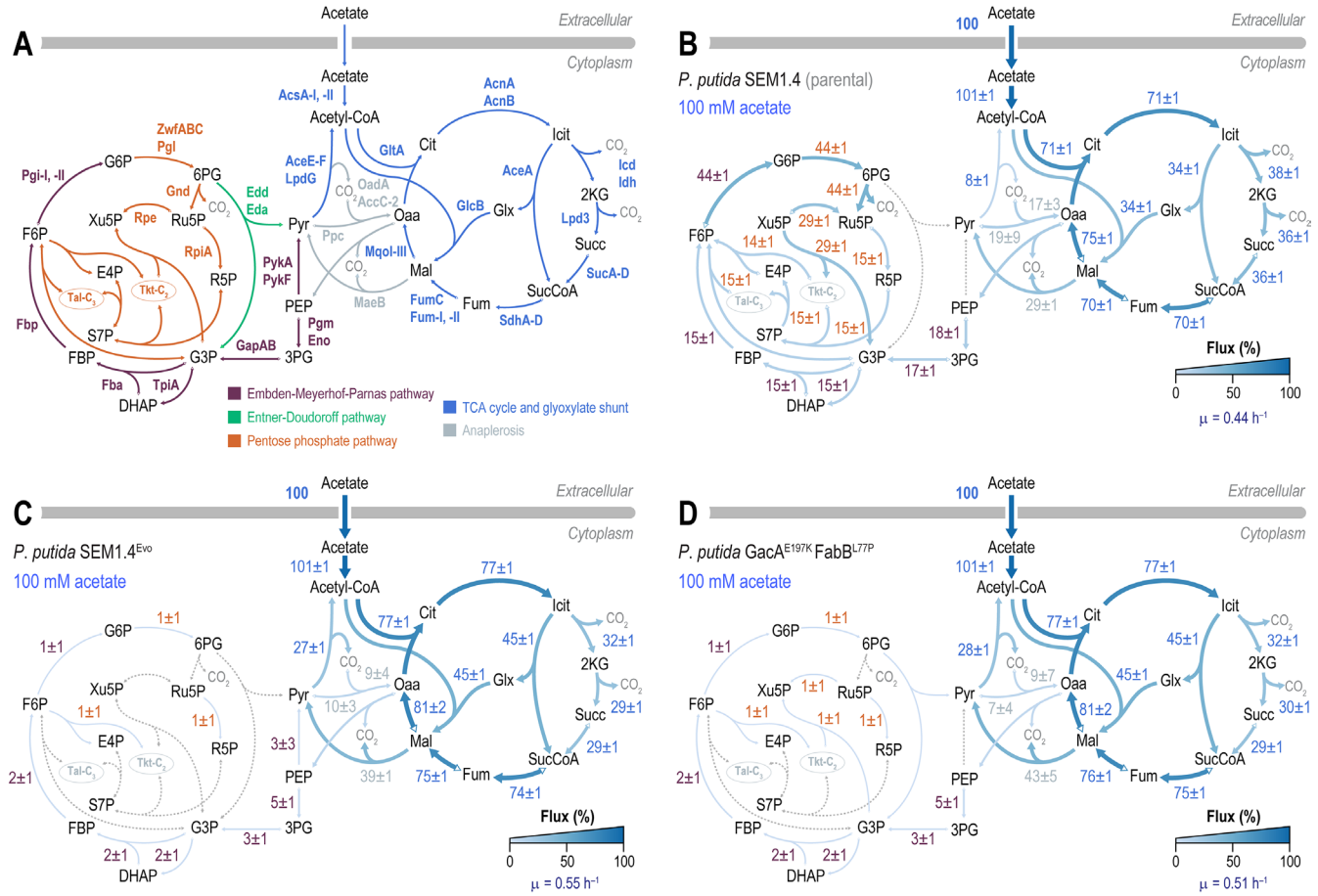


FIGURE 7 | Fluxomic analysis. Metabolic network of acetate assimilation and central carbon metabolism in *P. putida* KT2440, including the incomplete Embden-Meyerhof-Parnas pathway, Entner-Doudoroff pathway, pentose phosphate pathway, tricarboxylic acid (TCA) cycle and glyoxylate shunt, and anaplerotic and gluconeogenic reactions (A). In vivo carbon flux distributions in *P. putida* SEM1.4 (B), SEM1.4^{Evo} (C), and the reverse-engineered GacA^{E197K} FabB^{L77P} strain (D) during growth in MSM containing 5 g L^{-1} MOPS and supplemented with 100 mM acetate. Fluxes are expressed as percentages of the specific rate of acetate uptake (normalised to 100%), and values indicate mean fluxes ±95% confidence intervals from three independent tracer experiments. Arrow colour and thickness indicate relative flux magnitude according to the blue scale, whereas grey dashed lines indicate reactions for which no flux was detected. Specific growth rates (μ) are indicated for each strain. Some biochemical reactions are lumped, and not all enzymes, cofactors, or by-products are shown for clarity. 2KG, 2-ketoglutarate; 3PG, 3-phosphoglycerate; 6PG, 6-phosphogluconate; Acetyl-CoA, acetyl-coenzyme A; Cit, citrate; DHAP, dihydroxyacetone phosphate; E4P, erythrose-4-phosphate; F6P, fructose-6-phosphate; FBP, fructose-1,6-bisphosphate; Fum, fumarate; G3P, glyceraldehyde-3-phosphate; G6P, glucose-6-phosphate; Glx, glyoxylate; Icit, isocitrate; Mal, malate; Oaa, oxaloacetate; PEP, phosphoenolpyruvate; Pyr, pyruvate; R5P, ribose-5-phosphate; Ru5P, ribulose-5-phosphate; S7P, sedoheptulose-7-phosphate; Succ, succinate; SuccCoA, succinyl-coenzyme A; Xu5P, xylulose-5-phosphate.

gluconeogenesis and biomass synthesis (Turlin et al. 2025). The evolved and reverse-engineered strains also showed increased pyruvate-shunt flux relative to the parental strain, suggesting an additional route to balance redox metabolism while maintaining growth-supporting carbon fluxes (Chavarría et al. 2012, 2016).

These fluxomic results provide an independent mechanistic explanation for the higher biomass yields observed in strain SEM1.4^{Evo} and the reverse-engineered strain. The parental strain SEM1.4 consumed acetate faster but routed more carbon through stress-associated and cyclic metabolic activity, whereas the adapted strains consumed acetate more efficiently and retained more carbon in biomass. Together with transcriptomic repression of T6SS and carbohydrate storage genes, and proteomic reduction of oxidative stress-associated enzymes, the ^{13}C-MFA data support a model in which the *gacA*^{E197K} and *fabB*^{L77P} mutations reduce costly stress-associated expenditure and redirect acetate carbon toward biomass formation. Acetate tolerance in the evolved background is therefore associated with more efficient carbon use, as substantiated by higher biomass yields despite lower acetate uptake rates than those of the parental strain.

4 | Conclusion

Acetate is an attractive C_2 substrate for microbial bioproduction (Kiefer et al. 2021), but toxicity, redox imbalance and the ATP cost of activation can constrain the utilisation of this feedstock at elevated concentrations (Wolfe 2005; Trček et al. 2015). This study combined ALE, quantitative physiology, reverse engineering, transcriptomics, proteomics and ^{13}C-MFA to investigate substrate adaptation in a genome-reduced *P. putida*. The evolved and reverse-engineered strains achieved higher biomass

17517915, 2026, 10, Downloaded from https://environmicro-journals.onlinelibrary.wiley.com/doi/10.1111/1751-7915.70459 by Universitatsbibliothek RWTH Aachen University, Wiley Online Library on [13/11/2026]. See the Terms and Conditions (https://onlinelibrary.wiley.com/terms-and-conditions) on Wiley Online Library for rules of use; OA articles are governed by the applicable Creative Commons License

yields with lower specific acetate uptake rates, identifying improved conversion efficiency as a central feature of the adapted phenotype.

Reconstruction of the *gacA*^{E197K} and *fabB*^{L77P} mutations in the parental SEM1.4 background reproduced much of the evolved phenotype, including shorter lag phases, improved specific growth rates and higher biomass yields. These substitutions helped connect adaptation to global regulation and fatty acid metabolism. The GacS/GacA system controls secretion, motility, stress responses and secondary metabolism in *Pseudomonas* (Hassan et al. 2010; Song et al. 2023). Attenuation of this system offers a plausible route to reduce investment in selected cellular functions, consistent with adaptations reported during evolution on aromatic substrates (Mohamed et al. 2020; Bleem et al. 2024; Werner et al. 2025). The *fabB* substitution additionally implicates a role for lipid metabolism and membrane physiology (Hoang and Schweizer 1997; Yadrykhins'ky et al. 2021) in the evolved phenotype, although the individual molecular effects of the two substitutions remain unresolved. Complementary work by Filbig et al. (2026) identified GacS/GacA as an adaptive target in wild-type *P. putida* KT2440 and evaluated acetate-derived production of 3-(3-hydroxyalkanoyloxy) alkanoic acids. The convergence across strain backgrounds supports the relevance of this regulatory axis for acetate-based bioproduction.

These findings are consistent with the "fear versus greed" framework, in which growth-selected populations reduce investment in environmental defence programs while reallocating resources toward proliferation (Utrilla et al. 2016; Tan et al. 2020; Dalldorf et al. 2024). The acetate-adapted *P. putida* strains displayed a related pattern of reduced expression of selected secretion, storage, stress-associated and lipid metabolism functions. Together with increased biomass yield, these observations support the notion that resource reallocation is an integral part of the evolved phenotype.

Agreement between the transcriptomic and proteomic responses strengthened this interpretation, particularly for repressed functions. T6SS repression is relevant given the biosynthetic and energetic demands of this machinery (Bernal et al. 2017), while reduced expression of glycogen-, trehalose- and maltose-associated functions indicates altered investment in reserve carbohydrate metabolism. Lower abundance of oxidative stress-associated proteins is consistent with a reduced requirement for stress compensation. Changes in sulphur metabolism and reduced abundance of β-oxidation-associated proteins further suggest altered metabolic demands and acetyl-CoA allocation (Fujita et al. 2007). The multi-omic datasets therefore support coordinated functional changes while retaining differences between individual transcript and protein responses.

Flux analysis connected these expression patterns to central carbon redistribution. Pentose phosphate pathway fluxes were reduced in the adapted strains. These routes can support redox balancing and precursor supply under stress (Nikel et al. 2021), and their attenuation indicates a change in metabolic requirements. Increased relative glyoxylate-shunt flux provided a complementary carbon-conserving response through bypassing the CO_2-generating steps of the TCA cycle (Turlin et al. 2022). Together, the expression and flux profiles support a model in which regulatory and metabolic reorganisation contributed to improved biomass formation per unit of acetate consumed.

The use of *P. putida* SEM1.4 established the relevance of the identified adaptations in a genome-reduced production *chassis*. Genome reduction simplifies cellular architecture and can expose adaptation routes that improve growth and resource allocation under defined selective pressures. The acetate-tolerant *P. putida* derivatives generated here provide targets for further engineering of regulatory functions, fatty acid metabolism and central carbon allocation. Combining these adaptations with product-forming pathways could improve the use of acetate derived from biomass conversion, syngas fermentation, microbial electrosynthesis, or mixed-carbon waste streams (Kim et al. 2021). Finally, testing whether the observed increase in biomass yields translates into improved product yields represents a practical next step toward more carbon-efficient, acetate-based bioprocesses.

Author Contributions

Nicolás Gurdo: conceptualization, methodology, investigation, formal analysis, validation, visualization, data curation, writing – original draft, writing – review and editing. **Aparajitha Srinivasan:** methodology, investigation, formal analysis, data curation, validation, writing – review and editing. **Tommaso Tagliani:** formal analysis, investigation, methodology. **Melanie Filbig:** investigation, methodology. **Nicolas T. Wirth:** methodology, software, formal analysis, validation, data curation. **Josefin Johnsen:** investigation, methodology. **Garret W. O'Connell:** investigation. **Stefano Donati:** formal analysis, methodology. **Enrico Orsi:** methodology, formal analysis, data curation, validation. **María V. G. Alván-Vargas:** investigation. **Yan Chen:** methodology. **Christopher J. Petzold:** methodology. **Matthew Blow:** methodology, resources, data curation, validation. **Thomas Eng:** resources, supervision, data curation, validation, writing – review and editing. **Till Tiso:** methodology. **Lars M. Blank:** resources, supervision. **Adam Feist:** methodology, resources, supervision, funding acquisition. **Aindrila Mukhopadhyay:** conceptualization, resources, supervision, funding acquisition, project administration, writing – review and editing. **Pablo I. Nikel:** conceptualization, methodology, formal analysis, resources, supervision, funding acquisition, project administration, writing – review and editing.

Acknowledgements

The authors acknowledge the use of BioRender (https://biorender.com) for the creation of some schematic diagrams in this manuscript. The authors initially wrote the complete manuscript and used ChatGPT for English grammar checking. The authors then reviewed and revised the text to ensure accuracy. Financial support to P.I.N. was provided by the Novo Nordisk Foundation through *TARGET* (NNF21OC0067996), NNF20CC0035580 and BRIGHT (NNF24SA0100980), and by the European Union's Horizon 2020 Research and Innovation Programme under grant agreement 101082049 (*TOLERATE*). Part of this work was conducted at Lawrence Berkeley National Laboratory (LBNL) as part of N.G.'s visit through the DTU Exchange Program for PhD students. A.S., T.E., Y.C., C.J.P. and A.M. at LBNL are supported by the DOE Joint BioEnergy Institute (http://www.jbei.org), funded by the U.S. Department of Energy, Office of Science, Biological and Environmental Research Program, through contract DE-AC02-05CH11231 between Lawrence Berkeley National Laboratory and the U.S. Department of Energy. M.B. is supported by the U.S. Department of Energy Joint Genome Institute (https://ror.org/04xm1d337), a DOE Office of Science User Facility supported by the Office of Science of the U.S. Department of Energy and operated under Contract DE-AC02-05CH11231. The

17517915, 2026, 10, Downloaded from https://environmicro-journals.onlinelibrary.wiley.com/doi/10.1111/1751-7915.70459 by Universitatsbibliothek RWTH Aachen University, Wiley Online Library on [13/11/2026]. See the Terms and Conditions (https://onlinelibrary.wiley.com/terms-and-conditions) on Wiley Online Library for rules of use; OA articles are governed by the applicable Creative Commons License

RNA sequencing work (proposal https://doi.org/10.46936/10.25585/60001367 to T.E.) was conducted by the U.S. Department of Energy Joint Genome Institute (https://ror.org/04xm1d337), a DOE Office of Science User Facility supported by the Office of Science of the U.S. Department of Energy and operated under Contract DE-AC02-05CH11231. Any subjective views or opinions expressed in the paper do not necessarily represent the views of the U.S. Department of Energy or the United States Government.

Funding

This work was supported by Novo Nordisk Fonden, NNF21OC0067996, NNF20CC0035580, NNF24SA0100980; Horizon 2020 Framework Programme, 101082049; U.S. Department of Energy, DE-AC 02-05CH11231.

Conflicts of Interest

N.G., T.T. and P.I.N. are inventors on patent application WO20 25051835A1, which is assigned to the Technical University of Denmark and is partially based on results described in this manuscript. The other authors declare no conflicts of interest.

Data Availability Statement

All data used in this study are contained in the Data S1 file. Raw RNA-Seq data are available at the JGI Genome Portal (https://genome.jgi.doe.gov/portal) under project ID 1445921. The mass spectrometry proteomics data have been deposited to the ProteomeXchange Consortium via the PRIDE partner repository (Pérez-Riverol et al. 2022) under dataset ID PXD075741. The DIA-NN software is available at https://github.com/vdemichev/DiaNN.

References

Ackermann, Y. S., J. de Witt, M. P. Mezzina, et al. 2024. "Bio-Upcycling of Even and Uneven Medium-Chain-Length Diols and Dicarboxylates to Polyhydroxyalkanoates Using Engineered *Pseudomonas putida*." *Microbial Cell Factories* 23: 54.

Aguirre-Plans, J., A. Meseguer, R. Molina-Fernández, et al. 2021. "SPServer: Split-Statistical Potentials for the Analysis of Protein Structures and Protein-Protein Interactions." *BMC Bioinformatics* 22: 4.

Ahrné, E., Y. Ohta, F. Nikitin, A. Scherl, F. Lisacek, and M. Müller. 2011. "An Improved Method for the Construction of Decoy Peptide MS/MS Spectra Suitable for the Accurate Estimation of False Discovery Rates." *Proteomics* 11: 4085–4095.

Antoniewicz, M. R., J. K. Kelleher, and G. Stephanopoulos. 2006. "Determination of Confidence Intervals of Metabolic Fluxes Estimated From Stable Isotope Measurements." *Metabolic Engineering* 8: 324–337.

Bakker, E. P., and W. E. Mangerich. 1983. "The Effects of Weak Acids on Potassium Uptake by *Escherichia coli* K-12 Inhibition by Low Cytoplasmic pH." *Biochimica et Biophysica Acta* 730: 379–386.

Belda, E., R. G. A. van Heck, M. J. López-Sánchez, et al. 2016. "The Revisited Genome of *Pseudomonas putida* KT2440 Enlightens its Value as a Robust Metabolic *Chassis*." *Environmental Microbiology* 18: 3403–3424.

Bernal, P., L. P. Allsopp, A. Filloux, and M. A. Llamas. 2017. "The *Pseudomonas putida* T6SS is a Plant Warden Against Phytopathogens." *ISME Journal* 11: 972–987.

Bleem, A. C., E. Kuatsjah, J. Johnsen, et al. 2024. "Evolution and Engineering of Pathways for Aromatic *O*-Demethylation in *Pseudomonas putida* KT2440." *Metabolic Engineering* 84: 145–157.

Bujdoš, D., B. Popelářová, D. C. Volke, P. I. Nikel, N. Sonnenschein, and P. Dvořák. 2023. "Engineering of *Pseudomonas putida* for Accelerated Co-Utilization of Glucose and Cellobiose Yields Aerobic Overproduction of Pyruvate Explained by an Upgraded Metabolic Model." *Metabolic Engineering* 75: 29–46.

Bull, C. T., B. Duffy, C. Voisard, G. Défago, C. Keel, and D. Haas. 2001. "Characterization of Spontaneous *gacS* and *gacA* Regulatory Mutants of *Pseudomonas fluorescens* Biocontrol Strain CHA0." *Antonie van Leeuwenhoek* 79: 327–336.

Bushin, L. B., T. B. Alter, M. V. G. Alván-Vargas, et al. 2026. "Growth-Coupled Microbial Biosynthesis of the Animal Pigment Xanthommatin." *Nature Biotechnology* 44: 1525–1536.

Calero, P., N. Gurdo, and P. I. Nikel. 2022. "Role of the CrcB Transporter of *Pseudomonas putida* in the Multi-Level Stress Response Elicited by Mineral Fluoride." *Environmental Microbiology* 24: 5082–5104.

Calero, P., and P. I. Nikel. 2019. "Chasing Bacterial *Chassis* for Metabolic Engineering: A Perspective Review From Classical to Non-Traditional Microorganisms." *Microbial Biotechnology* 12: 98–124.

Cavaleiro, A. M., S. H. Kim, S. Seppälä, M. T. Nielsen, and M. H. Nørholm. 2015. "Accurate DNA Assembly and Genome Engineering With Optimized Uracil Excision Cloning." *ACS Synthetic Biology* 4: 1042–1046.

Chavarría, M., A. Goñi-Moreno, V. de Lorenzo, and P. I. Nikel. 2016. "A Metabolic Widget Adjusts the Phosphoenolpyruvate-Dependent Fructose Influx in *Pseudomonas putida*." *mSystems* 1: e00154-16.

Chavarría, M., R. J. Kleijn, U. Sauer, K. Pflüger-Grau, and V. de Lorenzo. 2012. "Regulatory Tasks of the Phosphoenolpyruvate-Phosphotransferase System of *Pseudomonas putida* in Central Carbon Metabolism." *mBio* 3: e00028–12.

Choe, D., J. H. Lee, M. Yoo, et al. 2019. "Adaptive Laboratory Evolution of a Genome-Reduced *Escherichia coli*." *Nature Communications* 10: 935.

Chong, H., J. Yeow, I. Wang, H. Song, and R. Jiang. 2013. "Improving Acetate Tolerance of *Escherichia coli* by Rewiring Its Global Regulator cAMP Receptor Protein (CRP)." *PLoS One* 8: e77422.

Czajka, J. J., D. Banerjee, T. Eng, et al. 2022. "Tuning a High Performing Multiplexed-CRISPRi *Pseudomonas putida* Strain to Further Enhance Indigoidine Production." *Metabolic Engineering Communications* 15: e00206.

Dalldorf, C., K. Rychel, R. Szubin, et al. 2024. "The Hallmarks of a Tradeoff in Transcriptomes That Balances Stress and Growth Functions." *mSystems* 9: e00305-24.

de Lorenzo, V., D. Pérez-Pantoja, and P. I. Nikel. 2024. "*Pseudomonas putida* KT2440: The Long Journey of a Soil-Dweller to Become a Synthetic Biology *Chassis*." *Journal of Bacteriology* 206: e00136–24.

Deatherage, D. E., and J. E. Barrick. 2014. "Identification of Mutations in Laboratory-Evolved Microbes From Next-Generation Sequencing Data Using Breseq." *Methods in Molecular Biology* 1151: 165–188.

Díaz-Guerra, M., M. Esteban, and J. L. Martínez. 1997. "Growth of *Escherichia coli* in Acetate as a Sole Carbon Source Is Inhibited by Ankyrin-Like Repeats Present in the 2′,5′-Linked Oligoadenylate-Dependent Human RNase L Enzyme." *FEMS Microbiology Letters* 149: 107–113.

Dragosits, M., and D. Mattanovich. 2013. "Adaptive Laboratory Evolution—Principles and Applications for Biotechnology." *Microbial Cell Factories* 12: 64.

Duffy, B. K., and G. Défago. 2000. "Controlling Instability in *gacS-gacA* Regulatory Genes During Inoculant Production of *Pseudomonas fluorescens* Biocontrol Strains." *Applied and Environmental Microbiology* 66: 3142–3150.

Dürre, P., and B. J. Eikmanns. 2015. "C_1-Carbon Sources for Chemical and Fuel Production by Microbial Gas Fermentation." *Current Opinion in Biotechnology* 35: 63–72.

Eng, T., D. Banerjee, A. K. Lau, et al. 2021. "Engineering *Pseudomonas putida* for Efficient Aromatic Conversion to Bioproduct Using High

17517915, 2026, 10, Downloaded from https://environmicro-journals.onlinelibrary.wiley.com/doi/10.1111/1751-7915.70459 by Universitatsbibliothek RWTH Aachen University, Wiley Online Library on [13/11/2026]. See the Terms and Conditions (https://onlinelibrary.wiley.com/terms-and-conditions) on Wiley Online Library for rules of use; OA articles are governed by the applicable Creative Commons License

Throughput Screening in a Bioreactor." *Metabolic Engineering* 66: 229–238.

Federici, F., F. Luppino, C. Aguilar-Vilar, et al. 2025. "CIFR (Clone-Integrate-Flip-Out-Repeat): A Toolset for Iterative Genome and Pathway Engineering of Gram-Negative Bacteria." *Metabolic Engineering* 88: 180–195.

Fernández-Cabezón, L., A. Cros, and P. I. Nikel. 2019. "Evolutionary Approaches for Engineering Industrially-Relevant Phenotypes in Bacterial Cell Factories." *Biotechnology Journal* 14: 1800439.

Fernández-Sandoval, M. T., G. Huerta-Beristain, B. Trujillo-Martinez, et al. 2012. "Laboratory Metabolic Evolution Improves Acetate Tolerance and Growth on Acetate of Ethanologenic *Escherichia coli* Under Non-Aerated Conditions in Glucose-Mineral Medium." *Applied Microbiology and Biotechnology* 96: 1291–1300.

Filbig, M., L. Wachtendonk, L. Hampe, et al. 2026. "Improving Acetate Metabolism of *P. putida* KT2440 by Evolutionary and Rational Engineering." *bioRxiv*: 746131. https://doi.org/10.64898/2026.08.21.746131.

Fujita, Y., H. Matsuoka, and K. Hirooka. 2007. "Regulation of Fatty Acid Metabolism in Bacteria." *Molecular Microbiology* 66: 829–839.

Genee, H. J., M. T. Bonde, F. O. Bagger, et al. 2015. "Software-Supported *USER* Cloning Strategies for Site-Directed Mutagenesis and DNA Assembly." *ACS Synthetic Biology* 4: 342–349.

Goedhart, J., and M. S. Luijsterburg. 2020. "VolcaNoseR Is a Web App for Creating, Exploring, Labeling and Sharing Volcano Plots." *Scientific Reports* 10: 20560.

Guan, N., and L. Liu. 2020. "Microbial Response to Acid Stress: Mechanisms and Applications." *Applied Microbiology and Biotechnology* 104: 51–65.

Gurdo, N., S. K. Taylor Parkins, M. Fricano, T. Wulff, L. K. Nielsen, and P. I. Nikel. 2023. "Protocol for Absolute Quantification of Proteins in Gram-Negative Bacteria Based on QconCAT-Based Labeled Peptides." *STAR Protocols* 4: 102060.

Hartmans, S., J. P. Smits, M. J. van der Werf, F. Volkering, and J. A. de Bont. 1989. "Metabolism of Styrene Oxide and 2-Phenylethanol in the Styrene-Degrading *Xanthobacter* Strain 124X." *Applied and Environmental Microbiology* 55: 2850–2855.

Hassan, K. A., A. Johnson, B. T. Shaffer, et al. 2010. "Inactivation of the GacA Response Regulator in *Pseudomonas fluorescens* Pf-5 has Far-Reaching Transcriptomic Consequences." *Environmental Microbiology* 12: 899–915.

Hoang, T. T., and H. P. Schweizer. 1997. "Fatty Acid Biosynthesis in *Pseudomonas aeruginosa*: Cloning and Characterization of the *fabAB* Operon Encoding β-Hydroxyacyl-Acyl Carrier Protein Dehydratase (FabA) and β-Ketoacyl-Acyl Carrier Protein Synthase I (FabB)." *Journal of Bacteriology* 179: 5326–5332.

Horinouchi, T., and C. Furusawa. 2020. "Understanding Metabolic Adaptation by Using Bacterial Laboratory Evolution and Trans-Omics Analysis." *Biophysical Reviews* 12: 677–682.

Hua, S., Y. Wang, L. Wang, et al. 2024. "Regulatory Mechanisms of Acetic Acid, Ethanol and High Temperature Tolerances of Acetic Acid Bacteria During Vinegar Production." *Microbial Cell Factories* 23: 324.

Jumper, J., R. Evans, A. Pritzel, et al. 2021. "Highly Accurate Protein Structure Prediction With AlphaFold." *Nature* 596: 583–589.

Kahn, D., and G. Ditta. 1991. "Modular Structure of FixJ: Homology of the Transcriptional Activator Domain With the −35 Binding Domain of σ Factors." *Molecular Microbiology* 5: 987–997.

Kiefer, D., M. Merkel, L. Lilge, M. Henkel, and R. Hausmann. 2021. "From Acetate to Bio-Based Products: Underexploited Potential for Industrial Biotechnology." *Trends in Biotechnology* 39: 397–411.

Kiefer, P., E. Heinzle, O. Zelder, and C. Wittmann. 2004. "Comparative Metabolic Flux Analysis of Lysine-Producing *Corynebacterium glutamicum* Cultured on Glucose or Fructose." *Applied and Environmental Microbiology* 70: 229–239.

Kim, D., B. Langmead, and S. L. Salzberg. 2015. "HISAT: A Fast Spliced Aligner With Low Memory Requirements." *Nature Methods* 12: 357–360.

Kim, S., J. Ha, H. Lee, et al. 2019. "Role of *Pseudomonas aeruginosa* DesB in Adaptation to Osmotic Stress." *Journal of Food Protection* 82: 1278–1282.

Kim, Y., S. Lama, D. Agrawal, V. Kumar, and S. Park. 2021. "Acetate as a Potential Feedstock for the Production of Value-Added Chemicals: Metabolism and Applications." *Biotechnology Advances* 49: 107736.

Kirkpatrick, C., L. M. Maurer, N. E. Oyelakin, Y. N. Yoncheva, R. Maurer, and J. L. Slonczewski. 2001. "Acetate and Formate Stress: Opposite Responses in the Proteome of *Escherichia coli*." *Journal of Bacteriology* 183: 6466–6477.

Kohlstedt, M., and C. Wittmann. 2019. "GC-MS-Based ^{13}C Metabolic Flux Analysis Resolves the Parallel and Cyclic Glucose Metabolism of *Pseudomonas putida* KT2440 and *Pseudomonas aeruginosa* PAO1." *Metabolic Engineering* 54: 35–53.

Kozaeva, E., S. Volkova, M. R. A. Matos, et al. 2021. "Model-Guided Dynamic Control of Essential Metabolic Nodes Boosts Acetyl-Coenzyme A–Dependent Bioproduction in Rewired *Pseudomonas putida*." *Metabolic Engineering* 67: 373–386.

Kuang, Z., X. Yan, Y. Yuan, et al. 2024. "Advances in Stress-Tolerance Elements for Microbial Cell Factories." *Synthetic and Systems Biotechnology* 9: 793–808.

Kutuzova, S., P. Colaianni, H. Röst, et al. 2020. "SmartPeak Automates Targeted and Quantitative Metabolomics Data Processing." *Analytical Chemistry* 92: 15968–15974.

LaCroix, R. A., B. Ø. Palsson, and A. M. Feist. 2017. "A Model for Designing Adaptive Laboratory Evolution Experiments." *Applied and Environmental Microbiology* 83: e03115–16.

Lasko, D. R., N. Zamboni, and U. Sauer. 2000. "Bacterial Response to Acetate Challenge: A Comparison of Tolerance Among Species." *Applied Microbiology and Biotechnology* 54: 243–247.

Liao, Y., G. K. Smyth, and W. Shi. 2014. "featureCounts: An Efficient General Purpose Program for Assigning Sequence Reads to Genomic Features." *Bioinformatics* 30: 923–930.

Lieder, S., P. I. Nikel, V. de Lorenzo, and R. Takors. 2015. "Genome Reduction Boosts Heterologous Gene Expression in *Pseudomonas putida*." *Microbial Cell Factories* 14: 23.

Lim, H. G., J. H. Lee, M. H. Noh, and G. Y. Jung. 2018. "Rediscovering Acetate Metabolism: Its Potential Sources and Utilization for Biobased Transformation into Value-Added Chemicals." *Journal of Agricultural and Food Chemistry* 66: 3998–4006.

Love, M. I., W. Huber, and S. Anders. 2014. "Moderated Estimation of Fold Change and Dispersion for RNA-Seq Data With DESeq2." *Genome Biology* 15: 550.

Luli, G. W., and W. R. Strohl. 1990. "Comparison of Growth, Acetate Production, and Acetate Inhibition of *Escherichia coli* Strains in Batch and Fed-Batch Fermentations." *Applied and Environmental Microbiology* 56: 1004–1011.

Ma, S., T. Su, X. Lu, and Q. Qi. 2024. "Bacterial Genome Reduction for Optimal *Chassis* of Synthetic Biology: A Review." *Critical Reviews in Biotechnology* 44: 660–673.

Martínez-García, E., P. I. Nikel, T. Aparicio, and V. de Lorenzo. 2014. "*Pseudomonas* 2.0: Genetic Upgrading of *P. putida* KT2440 as an Enhanced Host for Heterologous Gene Expression." *Microbial Cell Factories* 13: 159.

17517915, 2026, 10, Downloaded from https://environmicro-journals.onlinelibrary.wiley.com/doi/10.1111/1751-7915.70459 by Universitatsbibliothek RWTH Aachen University, Wiley Online Library on [13/11/2026]. See the Terms and Conditions (https://onlinelibrary.wiley.com/terms-and-conditions) on Wiley Online Library for rules of use; OA articles are governed by the applicable Creative Commons License

Martino, R. A., D. C. Volke, A. H. Tenaglia, P. M. Tribelli, P. I. Nikel, and A. M. Smania. 2025. "Genetic Dissection of Cyclic Di-GMP Signalling in *Pseudomonas aeruginosa via* Systematic Diguanylate Cyclase Disruption." *Microbial Biotechnology* 18: e70137.

May, H. D., P. J. Evans, and E. V. LaBelle. 2016. "The Bioelectrosynthesis of Acetate." *Current Opinion in Biotechnology* 42: 225–233.

Mohamed, E. T., A. Z. Werner, D. Salvachúa, et al. 2020. "Adaptive Laboratory Evolution of *Pseudomonas putida* KT2440 Improves *p*-Coumaric and Ferulic Acid Catabolism and Tolerance." *Metabolic Engineering Communications* 11: e00143.

Mordukhova, E. A., and J. G. Pan. 2013. "Evolved Cobalamin-Independent Methionine Synthase (MetE) Improves the Acetate and Thermal Tolerance of *Escherichia coli*." *Applied and Environmental Microbiology* 79: 7905–7915.

Nikel, P. I., M. Chavarría, T. Fuhrer, U. Sauer, and V. de Lorenzo. 2015. "*Pseudomonas putida* KT2440 Strain Metabolizes Glucose Through a Cycle Formed by Enzymes of the Entner-Doudoroff, Embden-Meyerhof-Parnas, and Pentose Phosphate Pathways." *Journal of Biological Chemistry* 290: 25920–25932.

Nikel, P. I., and V. de Lorenzo. 2013. "Implantation of Unmarked Regulatory and Metabolic Modules in Gram-Negative Bacteria With Specialised Mini-Transposon Delivery Vectors." *Journal of Biotechnology* 163: 143–154.

Nikel, P. I., and V. de Lorenzo. 2014. "Robustness of *Pseudomonas putida* KT2440 as a Host for Ethanol Biosynthesis." *New Biotechnology* 31: 562–571.

Nikel, P. I., and V. de Lorenzo. 2018. "*Pseudomonas putida* as a Functional *Chassis* for Industrial Biocatalysis: From Native Biochemistry to *Trans*-Metabolism." *Metabolic Engineering* 50: 142–155.

Nikel, P. I., T. Fuhrer, M. Chavarría, A. Sánchez-Pascuala, U. Sauer, and V. de Lorenzo. 2021. "Reconfiguration of Metabolic Fluxes in *Pseudomonas putida* as a Response to Sub-Lethal Oxidative Stress." *ISME Journal* 15: 1751–1766.

Nikel, P. I., M. J. Pettinari, M. C. Ramírez, M. A. Galvagno, and B. S. Méndez. 2008. "*Escherichia coli arcA* Mutants: Metabolic Profile Characterization of Microaerobic Cultures Using Glycerol as a Carbon Source." *Journal of Molecular Microbiology and Biotechnology* 15: 48–54.

Nikel, P. I., J. Zhu, K. Y. San, B. S. Méndez, and G. N. Bennett. 2009. "Metabolic Flux Analysis of *Escherichia coli creB* and *arcA* Mutants Reveals Shared Control of Carbon Catabolism Under Microaerobic Growth Conditions." *Journal of Bacteriology* 191: 5538–5548.

Nogales, J., J. Mueller, S. Gudmundsson, et al. 2020. "High-Quality Genome-Scale Metabolic Modelling of *Pseudomonas putida* Highlights Its Broad Metabolic Capabilities." *Environmental Microbiology* 22: 255–269.

Novak, K., and S. Pflügl. 2018. "Towards Biobased Industry: Acetate as a Promising Feedstock to Enhance the Potential of Microbial Cell Factories." *FEMS Microbiology Letters* 365: fny226.

Pardo, I., D. Bednar, P. Calero, D. C. Volke, J. Damborský, and P. I. Nikel. 2022. "A Nonconventional Archaeal Fluorinase Identified by *In Silico* Mining for Enhanced Fluorine Biocatalysis." *ACS Catalysis* 12: 6570–6577.

Paysan-Lafosse, T., M. Blum, S. Chuguransky, et al. 2023. "InterPro in 2022." *Nucleic Acids Research* 51: D418–D427.

Pérez-Riverol, Y., J. Bai, C. Bandla, et al. 2022. "The PRIDE Database Resources in 2022: A Hub for Mass Spectrometry-Based Proteomics Evidences." *Nucleic Acids Research* 50: D543–D552.

Phaneuf, P. V., D. Gosting, B. Ø. Palsson, and A. M. Feist. 2019. "*ALEdb 1.0*: A Database of Mutations From Adaptive Laboratory Evolution Experimentation." *Nucleic Acids Research* 47: D1164–D1171.

Pinhal, S., D. Ropers, J. Geiselmann, and H. de Jong. 2019. "Acetate Metabolism and the Inhibition of Bacterial Growth by Acetate." *Journal of Bacteriology* 201: e00147-19.

Puiggené, Ò., J. Muñoz-Triviño, L. Civil-Ferrer, et al. 2025. "Systematic Engineering of Synthetic Serine Cycles in *Pseudomonas putida* Uncovers Emergent Topologies for Methanol Assimilation." *Trends in Biotechnology* 43: 2539–2565.

Rajaraman, E., A. Agrawal, J. Crigler, R. Seipelt-Thiemann, E. Altman, and M. A. Eiteman. 2016. "Transcriptional Analysis and Adaptive Evolution of *Escherichia coli* Strains Growing on Acetate." *Applied Microbiology and Biotechnology* 100: 7777–7785.

Ramírez, F., F. Dündar, S. Diehl, B. A. Grüning, and T. Manke. 2014. "*deepTools*: A Flexible Platform for Exploring Deep-Sequencing Data." *Nucleic Acids Research* 42: W187–W191.

Roe, A. J., D. McLaggan, I. Davidson, C. O'Byrne, and I. R. Booth. 1998. "Perturbation of Anion Balance During Inhibition of Growth of *Escherichia coli* by Weak Acids." *Journal of Bacteriology* 180: 767–772.

Roe, A. J., C. O'Byrne, D. McLaggan, and I. R. Booth. 2002. "Inhibition of *Escherichia coli* Growth by Acetic Acid: A Problem With Methionine Biosynthesis and Homocysteine Toxicity." *Microbiology* 148: 2215–2222.

Sandberg, T. E., C. J. Lloyd, B. Ø. Palsson, and A. M. Feist. 2017. "Laboratory Evolution to Alternating Substrate Environments Yields Distinct Phenotypic and Genetic Adaptive Strategies." *Applied and Environmental Microbiology* 83: e00410-17.

Sandberg, T. E., M. J. Salazar, L. L. Weng, B. Ø. Palsson, and A. M. Feist. 2019. "The Emergence of Adaptive Laboratory Evolution as an Efficient Tool for Biological Discovery and Industrial Biotechnology." *Metabolic Engineering* 56: 1–16.

Schrader, J., M. Schilling, D. Holtmann, et al. 2009. "Methanol-Based Industrial Biotechnology: Current Status and Future Perspectives of Methylotrophic Bacteria." *Trends in Biotechnology* 27: 107–115.

Seong, W., G. H. Han, H. S. Lim, et al. 2020. "Adaptive Laboratory Evolution of *Escherichia coli* Lacking Cellular Byproduct Formation for Enhanced Acetate Utilization Through Compensatory ATP Consumption." *Metabolic Engineering* 62: 249–259.

Silva, J. C., R. Denny, C. Dorschel, et al. 2006. "Simultaneous Qualitative and Quantitative Analysis of the *Escherichia coli* Proteome: A *SWEET* Tale." *Molecular & Cellular Proteomics* 5: 589–607.

Sitnikov, D. M., J. B. Schineller, and T. O. Baldwin. 1995. "Transcriptional Regulation of Bioluminesence Genes From *Vibrio fischeri*." *Molecular Microbiology* 17: 801–812.

Song, H., Y. Li, and Y. Wang. 2023. "Two-Component System GacS/GacA, a Global Response Regulator of Bacterial Physiological Behaviors." *Engineering Microbiology* 3: 100051.

Szklarczyk, D., R. Kirsch, M. Koutrouli, et al. 2023. "The STRING Database in 2023: Protein-Protein Association Networks and Functional Enrichment Analyses for Any Sequenced Genome of Interest." *Nucleic Acids Research* 51: D638–D646.

Tan, J., A. V. Sastry, K. S. Fremming, et al. 2020. "Independent Component Analysis of *E. coli's* Transcriptome Reveals the Cellular Processes That Respond to Heterologous Gene Expression." *Metabolic Engineering* 61: 360–368.

Trček, J., N. P. Mira, and L. R. Jarboe. 2015. "Adaptation and Tolerance of Bacteria Against Acetic Acid." *Applied Microbiology and Biotechnology* 99: 6215–6229.

Turlin, J., M. V. G. Alván-Vargas, Ò. Puiggené, S. Donati, S. Wenk, and P. I. Nikel. 2025. "Synthetic C_1 Metabolism in *Pseudomonas putida* Enables Strict Formatotrophy and Methylotrophy *via* the Reductive Glycine Pathway." *mBio* 16: 01976–25.

Turlin, J., B. Dronsella, A. De Maria, S. N. Lindner, and P. I. Nikel. 2022. "Integrated Rational and Evolutionary Engineering of

17517915, 2026, 10, Downloaded from https://environmicro-journals.onlinelibrary.wiley.com/doi/10.1111/1751-7915.70459 by Universitatsbibliothek RWTH Aachen University, Wiley Online Library on [13/11/2026]. See the Terms and Conditions (https://onlinelibrary.wiley.com/terms-and-conditions) on Wiley Online Library for rules of use; OA articles are governed by the applicable Creative Commons License

Genome-Reduced *Pseudomonas putida* Strains Promotes Synthetic Formate Assimilation." *Metabolic Engineering* 74: 191–205.

Turlin, J., Ò. Puiggené, S. Donati, N. T. Wirth, and P. I. Nikel. 2023. "Core and Auxiliary Functions of One-Carbon Metabolism in *Pseudomonas putida* Exposed by a Systems-Level Analysis of Transcriptional and Physiological Responses." *mSystems* 8: e00004-23.

Utrilla, J., E. J. O'Brien, K. Chen, et al. 2016. "Global Rebalancing of Cellular Resources by Pleiotropic Point Mutations Illustrates a Multi-Scale Mechanism of Adaptive Evolution." *Cell Systems* 2: 260–271.

van den Broek, D., T. F. C. Chin-A-Woeng, G. V. Bloemberg, and B. J. J. Lugtenberg. 2005. "Molecular Nature of Spontaneous Modifications in *gacS* Which Cause Colony Phase Variation in *Pseudomonas* sp. Strain PCL1171." *Journal of Bacteriology* 187: 593–600.

Viana de Siqueira, G. M., T. Eng, A. Mukhopadhyay, and M. E. Guazzaroni. 2025. "Differences in GenBank and RefSeq Annotations May Affect Genomics Data Interpretation for *Pseudomonas putida* KT2440." *mSphere* 10: e00391-25.

Volke, D. C., P. Calero, and P. I. Nikel. 2020. "*Pseudomonas putida*." *Trends in Microbiology* 28: 512–513.

Volke, D. C., L. Friis, N. T. Wirth, J. Turlin, and P. I. Nikel. 2020. "Synthetic Control of Plasmid Replication Enables Target- and Self-Curing of Vectors and Expedites Genome Engineering of *Pseudomonas putida*." *Metabolic Engineering Communications* 10: e00126.

Waterhouse, A., M. Bertoni, S. Bienert, et al. 2018. "*SWISS-MODEL*: Homology Modelling of Protein Structures and Complexes." *Nucleic Acids Research* 46: W296–W303.

Weimer, A., M. Kohlstedt, D. C. Volke, P. I. Nikel, and C. Wittmann. 2020. "Industrial Biotechnology of *Pseudomonas putida*: Advances and Prospects." *Applied Microbiology and Biotechnology* 104: 7745–7766.

Wendisch, V. F., L. F. Brito, M. Gil-López, et al. 2016. "The Flexible Feedstock Concept in Industrial Biotechnology: Metabolic Engineering of *Escherichia coli*, *Corynebacterium glutamicum*, *Pseudomonas*, *Bacillus* and Yeast Strains for Access to Alternative Carbon Sources." *Journal of Biotechnology* 234: 139–157.

Werner, A. Z., Y. C. Avina, J. Johnsen, et al. 2025. "Adaptive Laboratory Evolution and Genetic Engineering Improved Terephthalate Utilization in *Pseudomonas putida* KT2440." *Metabolic Engineering* 88: 196–205.

Wiederstein, M., and M. J. Sippl. 2007. "ProSA-Web: Interactive Web Service for the Recognition of Errors in Three-Dimensional Structures of Proteins." *Nucleic Acids Research* 35: W407–W410.

Winsor, G. L., E. J. Griffiths, R. Lo, B. K. Dhillon, J. A. Shay, and F. S. Brinkman. 2016. "Enhanced Annotations and Features for Comparing Thousands of *Pseudomonas* Genomes in the *Pseudomonas* Genome Database." *Nucleic Acids Research* 44: D646–D653.

Wirth, N. T., J. Funk, S. Donati, and P. I. Nikel. 2023. "*QurvE*: User-Friendly Software for the Analysis of Biological Growth and Fluorescence Data." *Nature Protocols* 18: 2401–2403.

Wirth, N. T., E. Kozaeva, and P. I. Nikel. 2020. "Accelerated Genome Engineering of *Pseudomonas putida* by I-*Sce*I—Mediated Recombination and CRISPR-Cas9 Counterselection." *Microbial Biotechnology* 13: 233–249.

Wirth, N. T., K. Rohr, A. Danchin, and P. I. Nikel. 2023. "Recursive Genome Engineering Decodes the Evolutionary Origin of an Essential Thymidylate Kinase Activity in *Pseudomonas putida* KT2440." *mBio* 14: e01081-23.

Wolfe, A. J. 2005. "The Acetate Switch." *Microbiology and Molecular Biology Reviews* 69: 12–50.

Wynands, B., M. Otto, N. Runge, et al. 2019. "Streamlined *Pseudomonas taiwanensis* VLB120 *Chassis* Strains With Improved Bioprocess Features." *ACS Synthetic Biology* 8: 2036–2050.

Yadrykhins'ky, V., C. Georgiou, and R. Brenk. 2021. "Crystal Structure of *Pseudomonas aeruginosa* FabB C161A, a Template for Structure-Based Design for New Antibiotics." *F1000Research* 10: 74018.

Yan, Q., L. D. Lopes, B. T. Shaffer, et al. 2018. "Secondary Metabolism and Interspecific Competition Affect Accumulation of Spontaneous Mutants in the GacS-GacA Regulatory System in *Pseudomonas protegens*." *mBio* 9: e01845-18.

Young, J. D. 2014. "*INCA*: A Computational Platform for Isotopically Non-Stationary Metabolic Flux Analysis." *Bioinformatics* 30: 1333–1335.

Yus, E., T. Maier, K. Michalodimitrakis, et al. 2009. "Impact of Genome Reduction on Bacterial Metabolism and Its Regulation." *Science* 326: 1263–1268.

Zamboni, N., S. M. Fendt, M. Rühl, and U. Sauer. 2009. "^{13}C-Based Metabolic Flux Analysis." *Nature Protocols* 4: 878–892.

Zhang, J., Z. Liu, Y. Wang, and B. Yu. 2024. "Sustainable Production of L-Homoserine Solely From CO_2-Derived Acetate and Formate by Engineered *E. coli* Strain." *ACS Sustainable Chemistry & Engineering* 12: 18704–18711.

Supporting Information

Additional supporting information can be found online in the Supporting Information section. **Data S1:** Dataset 1.1: RNA-Seq data comparing the evolved strain versus the parental strain. **Dataset:** 1.2: RNA-Seq data comparing the GacA^{E197K} FabB^{L77P} strain versus the parental strain. **Dataset:** 1.3: RNA-Seq data comparing the GacA^{E197K} FabB^{L77P} strain versus the evolved strain. **Dataset:** 2.1: Proteomics data comparing the evolved strain versus the parental strain. **Dataset:** 2.2: Proteomics data comparing the GacA^{E197K} FabB^{L77P} strain versus the parental strain. **Dataset:** 2.3: Proteomics data comparing the GacA^{E197K} FabB^{L77P} strain versus the evolved strain. **Dataset:** 3.1: Quantitative physiology parameters. **Dataset:** 3.2: Metabolic flux values. **Figure S1:** In silico structural analysis of the GacA protein of *P. putida*. Structural models of the GacA^{E197K} mutant (A) and wild-type GacA (B), centered on residue 197 and the surrounding amino acids. Key residues (i.e., Cys162, Gln163, Lys164, Thr193 and Glu197/Lys197) are highlighted in the diagram. The residue selected for mutational analysis is indicated by a black dashed circle. Structures were visualised using PyMOL. In the parental GacA model, Glu197 was positioned approximately 2.9–3.1 Å from Thr193, suggesting a potential local stabilising interaction. The E197K substitution reversed the side-chain charge and altered its modelled orientation. **Figure S2:** Transcript interaction network analysis of significantly (A) upregulated and (B) downregulated genes in the evolved strain compared with the parental strain. **Figure S3:** Transcript interaction network analysis of significantly (A) upregulated and (B) downregulated genes in strain GacA^{E197K} FabB^{L77P} compared with the parental strain. **Figure S4:** Protein interaction network analysis of significantly (A) upregulated and (B) downregulated proteins in the evolved strain compared with the parental strain. **Figure S5:** Protein interaction network analysis of significantly (A) upregulated and (B) downregulated proteins in strain GacA^{E197K} FabB^{L77P} compared with the parental strain. **Table S1:** Bacterial strains used in this study. **Table S2:** Plasmids used in this study. **Table S3:** Oligonucleotides used in this study. **Table S4:** Carbon atom transitions used for ^{13}C-metabolic flux analysis.

17517915, 2026, 10, Downloaded from https://environmicro-journals.onlinelibrary.wiley.com/doi/10.1111/1751-7915.70459 by Universitatsbibliothek RWTH Aachen University, Wiley Online Library on [13/11/2026]. See the Terms and Conditions (https://onlinelibrary.wiley.com/terms-and-conditions) on Wiley Online Library for rules of use; OA articles are governed by the applicable Creative Commons License